CR 134968

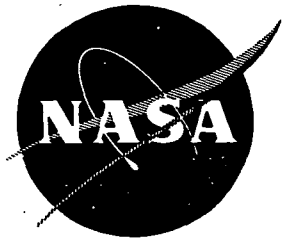

EPITAXIAL SOLAR CELL FABRICATION

BY

R. V. D'AIELLO, P. H. ROBINSON, AND H. KRESSEL

FINAL REPORT

DECEMBER 1975

PREPARED UNDER CONTRACT NAS3-19401

RCA LABORATORIES
PRINCETON, NEW JERSEY 08540

LEWIS RESEARCH CENTER
NATIONAL AERONAUTICS AND SPACE ADMINISTRATION
CLEVELAND, OHIO 44135

Clifford K. Swartz
Technical Monitor

NAS-3-19401
Lewis Research Center
NATIONAL AERONAUTICS AND SPACE ADMINISTRATION
Cleveland, Ohio 44135

Requests for copies of this report should be referred to:

NASA Scientific and Technical Information Facility
P. O. Box 33
College Park
Maryland 20740

1. Report No.	2. Government Accession No.	3. Recipient's Catalog No.
NASA CR-134968		

4. Title and Subtitle	5. Report Date
EPITAXIAL SOLAR CELL FABRICATION	December 1975
	6. Performing Organization Code
7. Author(s)	8. Performing Organization Report No.
R. V. D'Aiello, P. H. Robinson, and H. Kressel	PRRL-75-CR-73
9. Performing Organization Name and Address	10. Work Unit No.
RCA Laboratories Princeton, New Jersey 08540	11. Contract or Grant No. NAS3-19401
	13. Type of Report and Period Covered Contractor Report (11/11/74 to 11/10/75)
12. Sponsoring Agency Name and Address	14. Sponsoring Agency Code
National Aeronautics and Space Administration Washington, D.C. 20546	

15. Supplementary Notes

Technical Monitor, Clifford K. Swartz, NASA Lewis Research Center, Cleveland, Ohio 44135

16. Abstract

Silicon epitaxy has been studied for the fabrication of solar cell structures, with the intent of optimizing efficiency while maintaining suitability for space applications. Material properties were studied to ensure that the epitaxial method would produce Si layers and junctions that satisfy basic solar cell requirements. SiH_2Cl_2, a Si source material for the majority of structures investigated, yielded good-quality layers and junctions with reproducible impurity profiles. Diode characteristics and lifetimes in the epitaxial layers were investigated as a function of epitaxial growth conditions and doping profile, as was the effect of substrates and epitaxial post-gettering on lifetime. The pyrolytic decomposition of SiH_4 was also used in the epitaxial formation of highly doped junction layers on bulk Si wafers. The effects of junction layer thickness and bulk background doping level on cell performance, in particular, open-circuit voltage, were investigated. The most successful solar cells were fabricated with SiH_2 Cl_2 to grow p/n layers on n^+ substrates. The best performance was obtained from a $p^+/p/n/n^+$ structure grown with an exponential grade in the n-base layer. This cell had an AM-1 efficiency of 12.5% with V_{oc} = 636 mV measured at 29°C ± 2°C. The alternate approach of growing highly doped junctions on bulk silicon by the decomposition of silane was less successful. Degradation of V_{oc}, cell performance, and diode characteristics were found using this method.

17. Key Words (Selected by Author(s))	18. Distribution Statement
Solar cells Silicon epitaxy Epitaxial films Dichlorosilane	

19. Security Classif. (of this report)	20. Security Classif. (of this page)	21. No. of Pages	22. Price*
Unclassified	Unclassified	81	$3.00

*For sale by the Clearinghouse for Federal Scientific and Technical Information, Springfield, Virginia 22151.

TABLE OF CONTENTS

TABLE OF CONTENTS (Continued)

LIST OF ILLUSTRATIONS

LIST OF ILLUSTRATIONS (Continued)

LIST OF ILLUSTRATIONS (Continued)

EPITAXIAL SOLAR CELL FABRICATION

by

R. V. D'Aiello and P. H. Robinson

RCA Laboratories
Princeton, New Jersey 08540

SUMMARY

The use of silicon epitaxy has been studied for the fabrication of solar cell structures. The flexibility offered by this method was used to investigate solar cells having doping profiles designed to optimize efficiency while maintaining suitability for space applications. Material properties were first studied to ensure that the epitaxial method would produce silicon layers and junctions capable of satisfying the basic solar cell requirements. Dichlorosilane (SiH_2Cl_2) was used as the silicon source material for the majority of structures investigated and was found to yield good quality layers and junctions with reproducible impurity profiles.

Diode characteristics and lifetimes in the epitaxial layers were studied as a function of epitaxial growth conditions and doping profile. In addition, the effects of different substrates and epitaxial post-gettering on lifetime were investigated.

The pyrolytic decomposition of silane (SiH_4) was also used to study the epitaxial formation of highly doped junction layers on bulk silicon wafers. The effects of junction layer thickness and bulk background doping level on cell performance, particularly open-circuit voltage, were investigated.

The most successful solar cells were fabricated using dichlorosilane to grow p/n layers on n^+ substrates. The best performance was obtained from a $p^+/p/n/n^+$ structure grown with an exponential grade in the n-base layer. This cell had an AM-1 efficiency of 12.5%, with an open-circuit voltage of 636 mV measured at 29°C ±2°C. Other structures were studied and yielded good solar cell performance.

The alternate approach of growing highly doped junctions on bulk silicon by the decomposition of silane was less successful. Degradation of open-circuit voltage, cell performance, and diode characteristics were found using this method.

While it was found that record high open-circuit voltages, excellent junction characteristics, and good efficiency could be obtained by tailoring the doping profile using epitaxial techniques, further research is required to fully realize the potential of this method. Areas of further investigation should include:

(1) Base-layer gradients. An expanded study of the effect of gradients in the doping profile of base layers on solar cell performance.
(2) Surface layer profiles and gradients. A study of gradients grown epitaxially into the surface layer of n/p and p/n solar cell structures.
(3) Characterization of layer and junction defects. Identify impurities and defects in epitaxial layers which are related to limitations in solar cell performance. Specifically, methods should be developed to elucidate the mechanisms which limit lifetime and contribute to less than "ideal" junction characteristics.

I. INTRODUCTION

Traditionally, solar cells for space and terrestrial applications have been made by diffusion into bulk silicon (ref. 1). While improvements in the efficiency of these cells have been achieved (refs. 2,3), because of the nature of the diffusion process for very shallow junction depths, reproducibility is difficult and structural flexibility is limited. Epitaxial growth of the layers provides a method whereby the doping distribution and layer thickness can be readily adjusted to optimize the solar cell structure (ref. 4). In addition, thin epitaxial cells have been shown to be resistant to radiation damage associated with space applications (refs. 5,6).

The present research was undertaken with the objective of exploring the use of silicon epitaxy in the fabrication of solar cell structures. In particular, the effect of junction quality and doping profile on the solar cell parameters as open-circuit voltage, fill-factor, and efficiency were investigated. This work has included epitaxial layer materials characterization, lifetime and diode characteristic studies, and the fabrication and evaluation of solar cells grown by several epitaxial techniques.

This Final Report describes the research performed during the period 11 November 1974 to 10 November 1975.

The authors gratefully acknowledge the contributions to this research made by: J. Jacklick, J. Murr, D. Patterson, F. Tams III, D. Tarangioli, and R. Wance. We would also like to thank Dr. Y. S. Chiang for help in growing the silane layers.

II. BASIC MATERIAL AND JUNCTION REQUIREMENTS FOR EFFICIENT SOLAR CELL OPERATION

Aside from the fundamental losses associated with the conversion of photon energy to electric current and voltage in solar cells, and the losses related to such practical considerations as grid coverage and surface reflections, the major loss in efficiency of a solar cell can be attributed to the nonideal behavior of the junction current (ref. 7). This nonideal behavior can often be traced to defects and impurities related to high doping effects (ref. 8) in the bulk of the material or in the vicinity of the junction.

Quantitatively, the power output (P_{max}) of a solar cell can be expressed as

$$P_{max} = F.F. \times J_{sc} \times V_{oc} \tag{1}$$

where F.F. is the fill-factor, J_{sc} is the short-circuit current density, and V_{oc} is the cell open-circuit voltage. Obviously, each of these items should be maximized for optimum efficiency. Although these three parameters are not independent, they are all affected by the form of the current-voltage (I-V) characteristic associated with the junction used to collect the solar-generated current. In the ideal case, the junction current and voltage are related by the Shockley (ref. 9) equation:

$$J(V) = J_o[\exp V/nV_o - 1] - J_{sc} \tag{2}$$

where J_o = saturation current density

V_o = kT/q (thermal voltage)

n = 1 (ideal)

J_{sc} = solar-generated short-circuit current density.

For a symmetrical and uniformly doped p/n junction, semi-infinite in extent, and neglecting space charge currents generated in the depletion layers

$$J_o = q\, n_i^2 \left[\frac{1}{N_D}\sqrt{\frac{D_p}{\tau_p}} + \frac{1}{N_A}\sqrt{\frac{D_n}{\tau_n}}\right] \tag{3}$$

where

n_i = intrinsic carrier density for silicon

q = electron charge

$D_{n,p}$ = diffusivity for electrons, holes

$\tau_{n,p}$ = minority carrier lifetime for electrons, holes.

$N_{D,A}$ = doping density in n, p regions

From Eq. (1) the open-circuit voltage (V_{oc}) is:

$$V_{oc} = kT/q \ln \left[\frac{J_{sc}}{J_o} + 1\right] \tag{4}$$

To maximize V_{oc}, a low value of J_o and a high short-circuit current are required. From Eq. (3), minimizing J_o requires long lifetimes and high doping densities, a conflicting requirement in view of the generally observed decrease in lifetime with increasing doping level.

The value of J_o is also sensitive to the assumption of a semi-infinite cell structure, as the back contact or other back surface profile affects the flow of minority carriers, resulting in modifications to Eq. (3) (refs. 10, 11). These effects have been considered in the literature (ref. 12) where it is shown that substantial improvement in cell open-circuit voltage is observed for $n/p/p^+$ structures (back surface field cells).

For practical junctions, the I-V relationship, Eq. (2), generally takes the form:

$$J(V) = \sum_{i=2} J_i \left[\exp \frac{V}{n_i V_o} - 1\right] + J_{o1} \left[\exp \frac{(V-IR_s)}{n_1 V_o} - 1\right] - J_{sc} \tag{5}$$

where the terms associated with J_i are due, in part, to space charge generated currents, surface leakage, and shunting currents at localized defects. Also n_1 is generally greater than the ideal value of unity, and J_{o1} is higher than J_o.

A comparison of these I-V characteristics is shown in Fig. 1 where it can be seen that for a given short-circuit current density, the open-circuit voltage is lower for the nonideal case. In addition to lower V_{oc}, the nonideal I-V curve yields a lower fill-factor because in the region of voltage less than V_B, the current increases less rapidly with voltage due to the slope n_2.

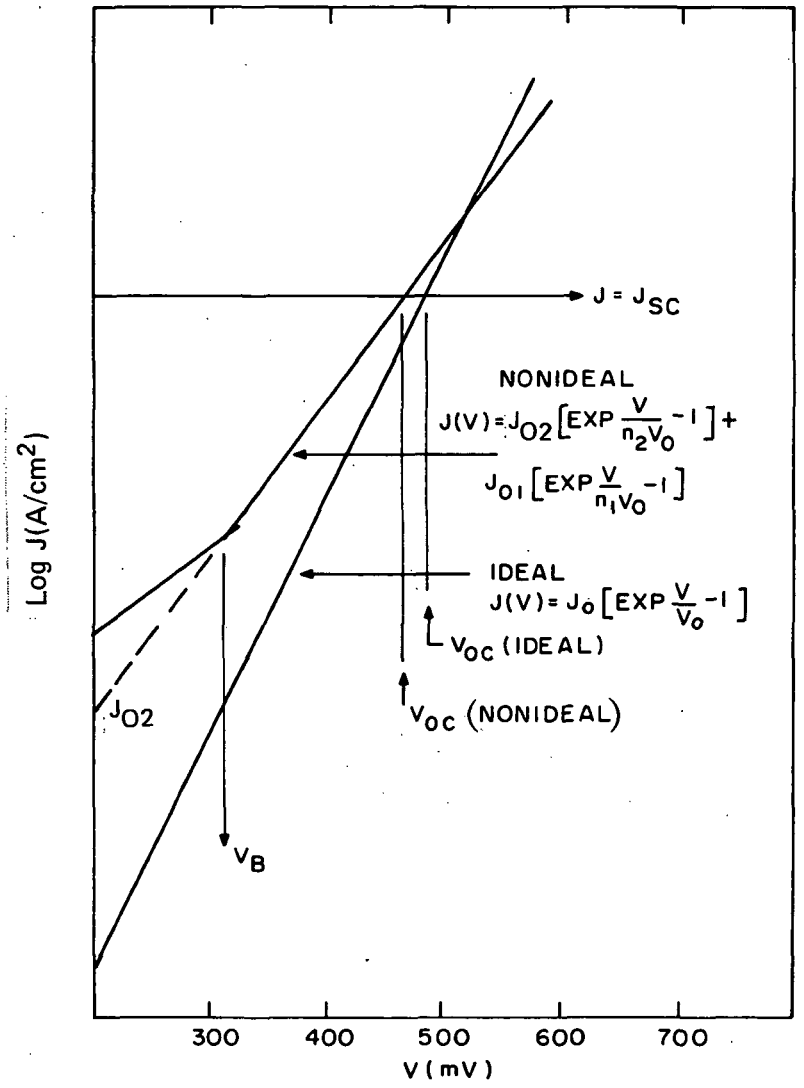

Figure 1. The effects of diode I-V characteristics on solar cell parameters.

The short-circuit current density (J_{sc}) of a solar cell is determined primarily by its quantum efficiency. If all the photons contained in the AM-1 solar spectrum between 0.4 and 1 μm were absorbed and converted to a photocurrent in a cell with 100% quantum efficiency, the result would be J_{sc} = 45 mA/cm^2. The achievement of this limit requires the following:

(1) Reduction in surface losses by having a low surface recombination velocity and reasonably long lifetime in the top layer. In addition, "dead zones" in the doping profile near the surface should be minimized.

(2) Active epitaxial layers of approximately 100-μm thickness, since reasonably strong absorption of photons of wavelength λ = 1.0 μm contribute to J_{sc}.

(3) The minority carrier diffusion length must then be at least 100 μm. This corresponds to a lifetime in p-layers, for example, of ∿5 μs.

If epitaxial layers are to be used in the fabrication of solar cells, the basic material and junction requirements for efficient cell performance are:

(1) The material must be relatively free of gross bulk defects which cause excess junction currents. Defect-free layers of ∿100-μm thickness are required.

(2) Junctions formed by the epitaxial process should yield near "ideal" I-V characteristics.

(3) Reasonably long lifetimes should be obtained in both p- and n-layers to provide good collection efficiency on both sides of the junction.

The above specifications are minimum requirements for the use of epitaxial methods in achieving high-efficiency solar cells. Additional benefits can be obtained from the epitaxial process by tailoring the doping profile to maximize the collection efficiency. For example, by epitaxy, it is relatively easy to grade the profile on one or both sides of the junction with the doping density increasing with distance away from the junction, providing a drift electric field which aids in collecting photogenerated carriers. Such profiles were grown and yielded an enhanced performance. These results are discussed in Section V-C.

III. EPITAXIAL TECHNIQUES

A. Apparatus and Techniques (Dichlorosilane)

In applying the epitaxial growth technique for the preparation of silicon layers, it is necessary to find a volatile silicon compound which is available in very high purity and can be reduced to elemental silicon using heat and hydrogen. The most widely used technology at present is based on the hydrogen reduction of either silicon tetrachloride or trichlorosilane at temperatures from 1100° to 1200°C. Both of these are liquids at room temperature, and are introduced into the reactor by sweeping a carrier gas either through or over the liquid to pick up a controlled amount of vapor. The concentration of the resulting gas mixture depends on the vapor pressure of the chlorosilane and the geometry of the vessel used to form the gas mixture. Since the vapor pressure is a strong function of temperature, elaborate methods must be employed to keep the concentration of the chlorosilane and, hence, the growth rate constant.

Dichlorosilane has recently become available commercially in a purity suitable for use as a source material for the epitaxial growth of silicon, and has several attributes which makes it attractive. At room temperature, it is a liquid with a vapor pressure of about 1.7 atm which means it can be metered directly into the gas stream with a great degree of accuracy. Furthermore, its overall reaction rate is very nearly independent of temperature in the normal range of temperatures used for epitaxial growth. This means that deposition temperatures can be selected which yield optimal control of dopant distribution without compromising on growth rate which should lead to improved control of both thickness and resistivity.

The growths were carried out using a horizontal reactor. The quartz tube has a cross section of 5 x 10 cm and held a silicon carbide-coated graphite susceptor that was 30.5 cm long. Heating was accomplished by rf induction into the susceptor, which was inclined horizontally, and the walls of the reactor were air-cooled. All the gases were metered into the system from a control panel which provided automatic timing of the deviation of each run. Hydrogen was obtained from a Pd-Ag diffusion cell. Doping gases were arsine or diborane diluted with hydrogen at the 10- to 20-ppm level and were further diluted as needed before they were metered into the reactant stream. Dichlorosilane was metered as a gas directly from the cylinder, and temperatures were measured with an optical pyrometer.

The substrates were either 1.5 or 2 in. in diameter, oriented 1.5 to 3° off the (111) plane toward the nearest (110) and were polished with

colloidal silica. They were cleaned prior to insertion into the epitaxial reactor using the method described by Kern and Puotinen (ref. 13) and were further cleaned, *in situ*, by etching with HCl gas just prior to growth. Most of the layers used in this work were grown at a rate of 5 μm/min; however, growth rates from 1 to ∿20 μm/min were investigated.

B. Epitaxial Growth Using Silane

For the studies of thin (submicron) layers grown on bulk silicon wafers, pyrolytic decomposition of silane was used in the epitaxial growth. For this application, the silane method was selected because doping levels in excess of 10^{19} cm^{-3} and growth of epitaxial layers down to ∿0.25 μm can be obtained with more control than with the dichlorosilane technique as it is used presently.

The silane layers were grown in a barrel reactor at a temperature of 1100°C. No HCl gas etching was done prior to the epitaxial growth. The growth rate was 0.4 μm/min and profile was graded from ∿5 x 10^{19} A/cm^3 at the surface to ∿10^{17} A/cm^3 at the junction. Junction layers of 0.3, 1, and 3 μm were grown on bulk n and p silicon wafers having resistivities ranging from 0.16 to 12 Ω-cm. For p-layers, boron (diborane) was used; the n-layers were grown using a combination of phosphine and arsine in atomic ratio of 4:1. After the layers were grown, the reactor was slow-cooled to 500°C at a rate of 10°C/min.

IV. CHARACTERIZATION OF EPITAXIAL LAYERS

To establish the suitability of the epitaxial method for the fabrication of solar cell structures, the junction and material quality must first be established. For this purpose, various layers containing a junction were grown with doping profiles and layer thicknesses similar to those required for solar cell structures. Spreading resistance techniques were used to characterize the layers for resistivity, thickness, and profile; mesa diodes were fabricated; lifetimes and diode I-V characteristics were measured. The results of these measurements in relation to the epitaxial growth parameters and the structure of the layers are given in this section.

A. Measurement of Epitaxial Layer Profiles Using Spreading Resistance

The use of spreading resistance for profile analysis of silicon structures is becoming an established technique in the semiconductor industry (refs. 14,15). In our laboratory we have used the Model ASR-100* during the past four years for the analysis of a variety of silicon devices and epitaxial structures.

The raw data output of our probe is digitized and punched on a paper tape. The data is then fed to a computer for correction and conversion to a concentration profile. Because of the nature of the sample preparation (lapped, bevel-surface), there is a noise factor of $\sim$10% rms on the concentration profiles.

Typical profiles for epitaxial structures intended to be uniform in doping are shown in Figs. 2 and 3. Reproducibility of doping level and thickness of such profiles was achieved well within %10%.

An important aspect of the work on solar cell structures involves the growth of graded profiles. Such a graded structure is shown in Fig. 4 where the grading structure is in the n-layer. This profile is achieved by manually adjusting the arsine flow meter as a prescribed function of time during the layer growth. Presently, we are experimenting with mass-flow controllers under digital control.

*Model ASR-100, Automatic Spreading Resistance Probe, Solid State Measurements, Inc., Monroeville, Pa. 15146.

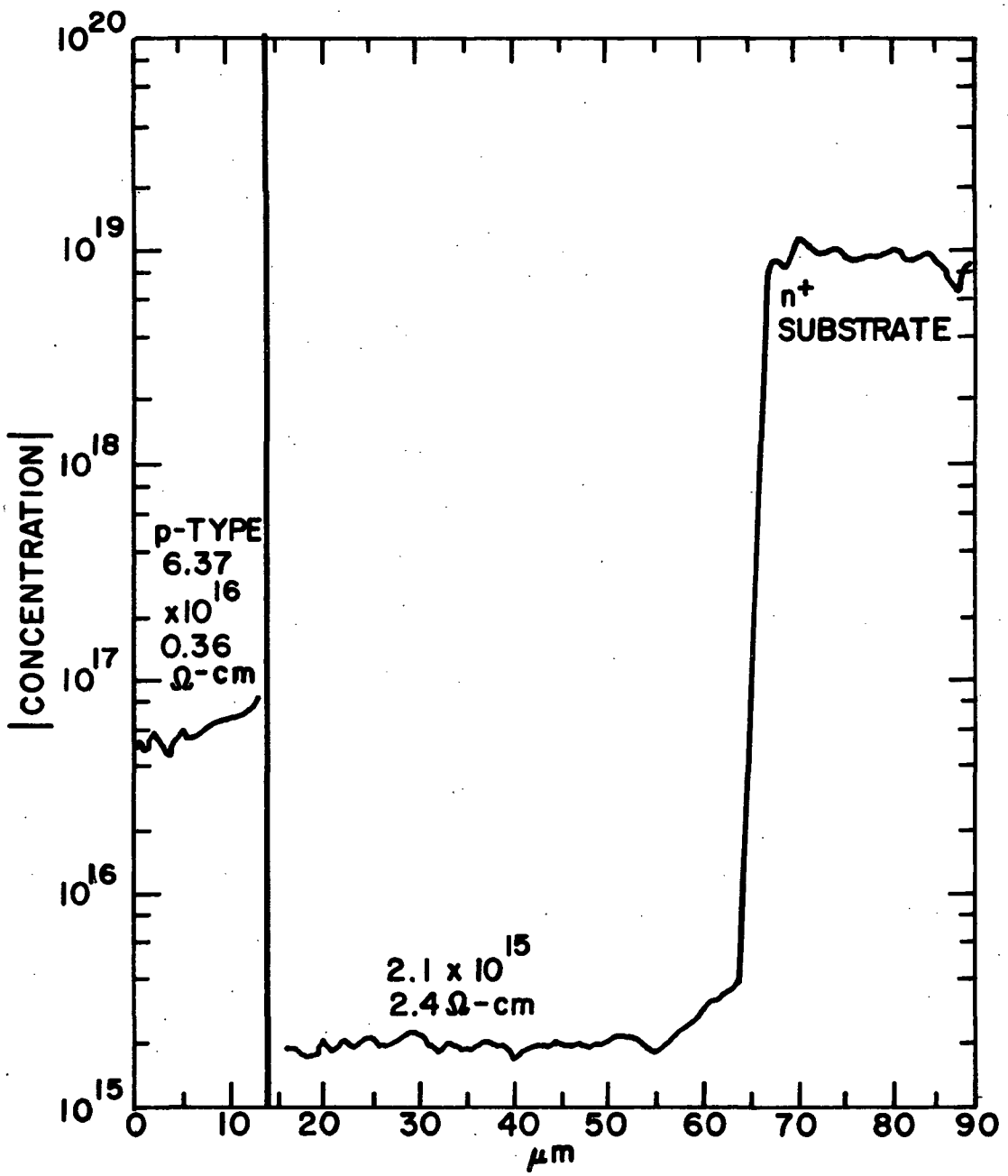

Figure 2. Typical doping profile of a p/n/n^+ epitaxial structure obtained from spreading resistance. Average n-layer doping = 1.8 x 10^{15} A cm^{-3}.

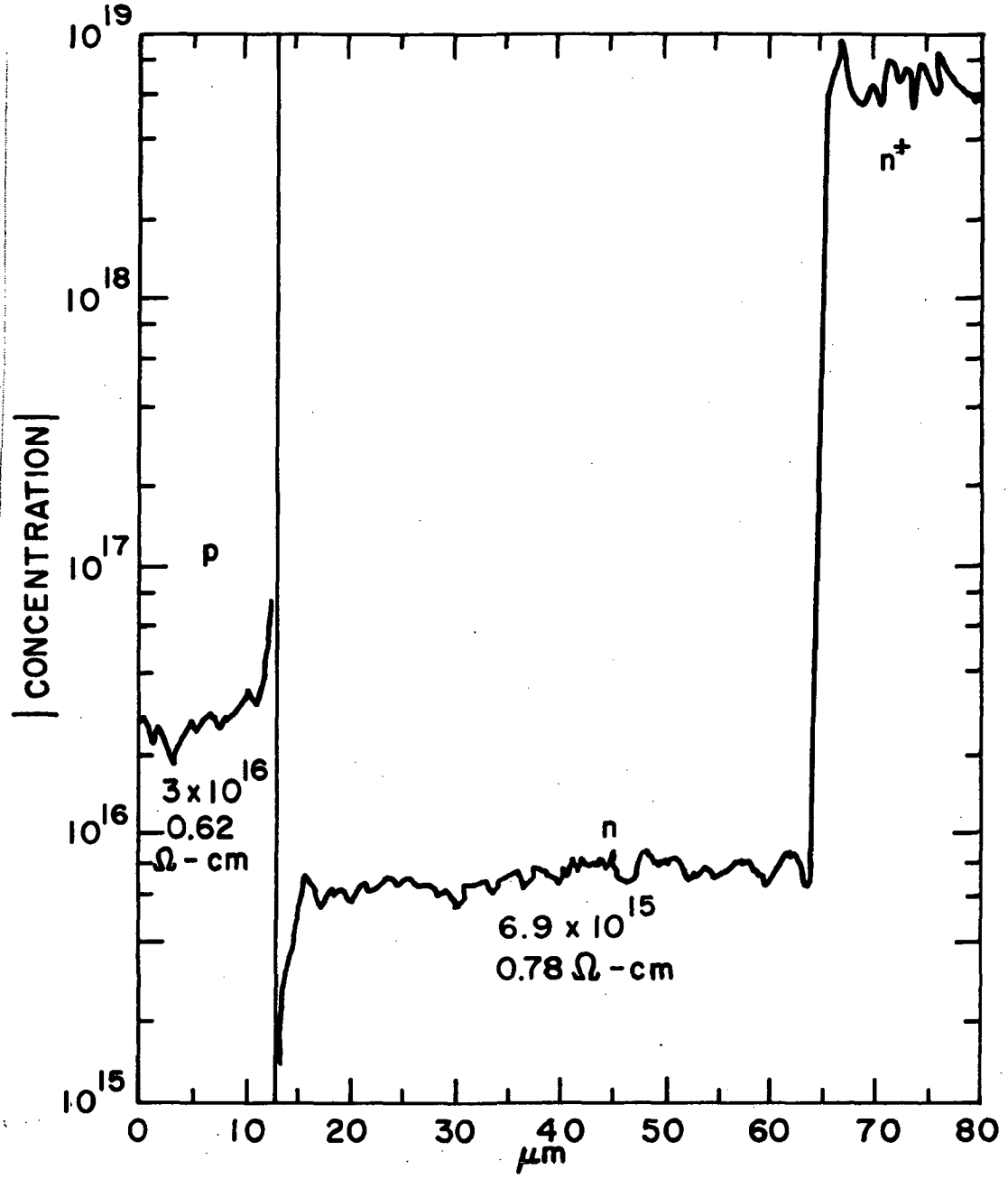

Figure 3. Typical doping profile of a p/n/n^+ epitaxial structure obtained from spreading resistance. Average n-layer doping = 6.9 x 10^{15} A cm^{-3}.

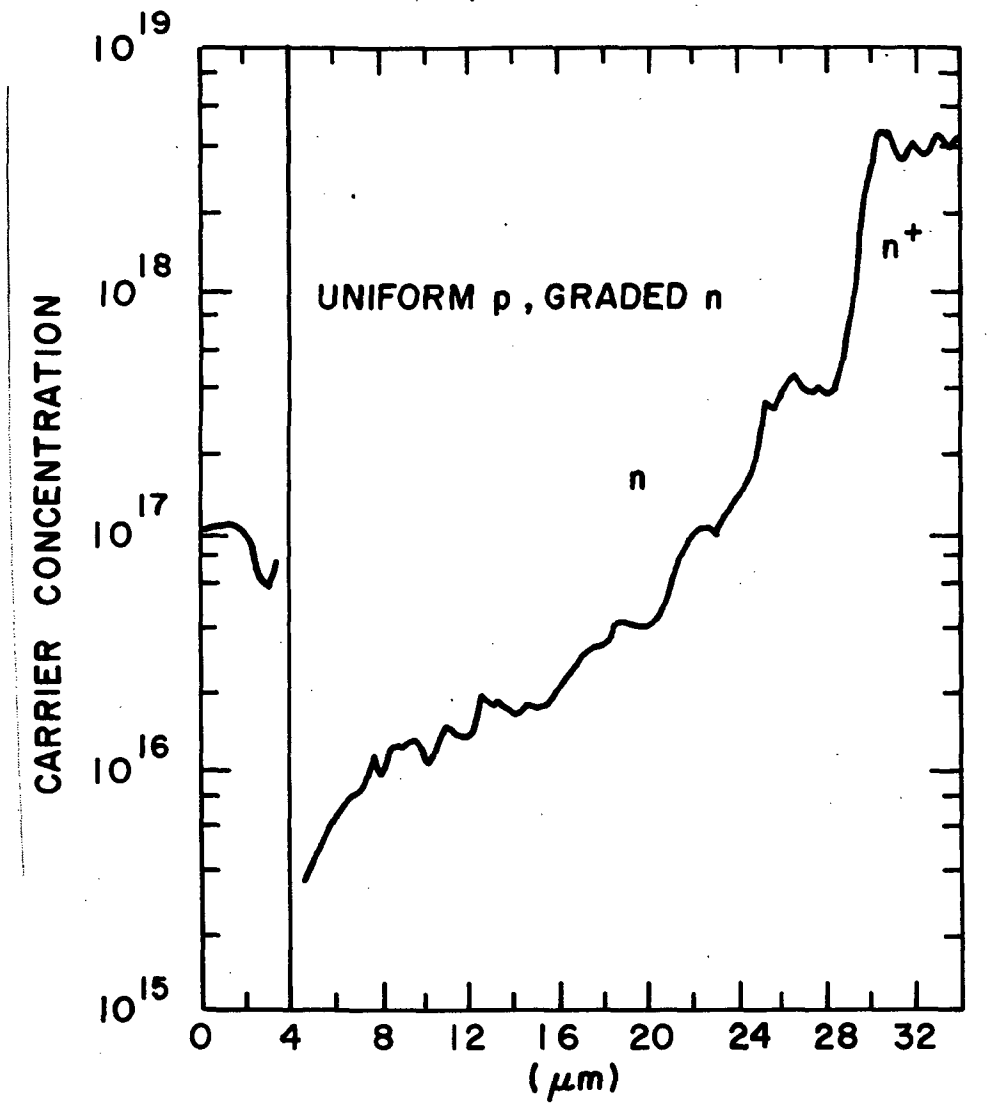

Figure 4. Doping profile of a p/n/n^+ epitaxial structure containing an intentionally graded n-layer.

B. Lifetime Related To Epitaxial Parameters

1. Lifetime As a Function of Silicon Source Material. - Three sources (tanks) of dichlorosilane were used to grow the following two structures to establish a baseline with regard to minority carrier lifetime.

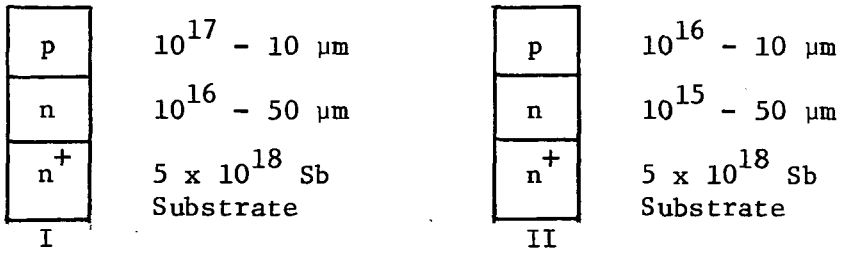

Mesa diodes were fabricated and the minority carrier lifetimes were measured by the pulsed, reverse recovery, and open-circuit voltage techniques described in Appendix B. The results of these measurements are shown in Table I.

TABLE I. COMPARISON OF MEASURED LIFETIMES FOR DIFFERENT TANKS OF DICHLOROSILANE AND DIFFERENT RESISTIVITY LEVELS

Tank - Structure	Lifetime (ns)
1 - II	480
1-- I	< 300
2 - II	2875
2 - I	1340
3 - II	3400
3 - I	1600

Tank 1 contains an unwanted impurity at sufficiently high concentrations to reduce the minority carrier lifetime significantly. Also, as expected, the lifetime decreases with increasing doping levels. This is the standard technique used on all new sources of dichlorosilane, as received, and all recent material has been determined to be at the 2- to 3-μs level.

2. Effect of Growth Rate on Lifetime. - The same 10^{16} to 10^{15} A/cm^3 p-on-n structure just described was grown at 0.75, 2, 5, 10, 16 μm/min and lifetimes measured. The lifetimes were found to be essentially constant over the 2- to 16-μm/min growth rate range and varied between 2 and 2.5 μs. At a growth rate of 0.75 μm/min, however, the lifetime dropped below 1 μs. It should be noted that the sample grown at 0.75 μm/min had poor cosmetics, which was due probably to the long time required to grow these layers at the low growth rate.

3. Effect of n-Layer Thickness on Lifetime. - The same structure was grown again, except the n-layer thickness was increased to 150 μm. The lifetimes show no significant difference from those obtained using 50-μm-thick n-layers. These data also suggest that the n/n^+ interface is not affecting the measured lifetime and that the lifetimes measured are characteristic of the epitaxial layers.

4. Gettering. - In an attempt to obtain longer lifetimes, several gettering techniques were applied to the $p/n/n^+$ structures.

For the gettering experiments, samples from our previous epitaxial runs having the shortest and the longest lifetime were selected. Each wafer was sliced into three parts, and a matrix of gettering techniques was performed to each wafer as follows:

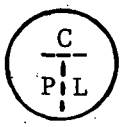

C = Control	No gettering
P = $POCl_3$[(a)]	1200°C/1 h/slow cool @ 2°C/min to 700°C
L = Lapped[(b)]	1200°C/1 h/slow cool @ 2°C/min to 700°C

After gettering, 40-mil-diameter mesa-type diodes were formed, having top (Al) and bottom (Cr/Ni) metallization. Lifetime was measured on these diodes using the reverse recovery and the open-circuit recovery techniques. The results of the analysis of these data are shown in Table II.

Several conclusions can be drawn from these data. First, gettering was ineffective on the low lifetime material, indicating that the lifetime killers in this sample are not heavy metals (i.e., Cu, Fe) since these are known to be reduced in concentration by phosphorus gettering (ref. 16). Second, gettering on the higher lifetime samples was effective, yielding a 45% increase in lifetime for the lapped sample and a 20% increase for the phosphorus-gettered sample. This indicates that as the ungetterable lifetime killers are reduced by improved epitaxial growth techniques, gettering will become more effective.

5. The Effect of Carrier Concentration in Active Layers and Substrates. - There have been reports (ref. 16) that an improvement in the minority carrier lifetime of epitaxial silicon layers can be obtained with the use of substrates heavily doped with phosphorus. We have observed this

(a) $POCl_3$ prediffusion into back of wafer at 1050°C for 20 min.
(b) Back of wafer lapped with silicon carbide grit (20 μm) to form dislocations which act as sinks for contaminants.

TABLE II. SUMMARY OF THE EFFECT OF GETTERING ON LIFETIME

Initial State	Low Lifetime Sample*		High Lifetime Sample*	
	τ_{RR} (ns)	τ_{oc} (ns)	τ_{RR} (ns)	τ_{oc} (ns)
Control Wafer	820	720	2100	1000
$POCl_3$-gettered	820	670	2500	2310
Lapped-back	550	520	3050	3340

*Both samples were $p/n/n^+$ epitaxial layers with 10 μm of p at $N_A = 1 \times 10^{16}$ A/cm^3 and a 50-μm n-layer with $N_D = 2 \times 10^{15}$ A/cm^3.

effect and have measured lifetimes as high as about 15 μs on epitaxial layers doped in the 10^{15} A/cm^3 range. Figure 5 shows a plot of minority carrier lifetime vs carrier concentration for 50-μm-thick epitaxial layers on antimony-, phosphorus-, and arsenic-doped substrates. The best epitaxial solar cell performance obtained to date has been with phosphorus-doped n^{++} substrates.

C. Diode I-V Characteristics

The exact form of the forward I-V characteristic plays an important role in determining solar cell efficiency. Accordingly, the I-V characteristics of diodes made from epitaxial $p/n/n^+$ and $n/p/p^+$ structures were studied in detail.

The diodes were prepared by first metallizing both sides of each wafer: aluminum on the side closest to the junction, and chromium/nickel on the back. Mesa diodes 0.036 in. in diameter were formed by etching 2 mils deep into the silicon using a 40-mil-diameter wax mask. The diodes were then separated by scribing, soldered onto headers (TO-5), and ultrasonically bonded using a 2-mil aluminum wire.

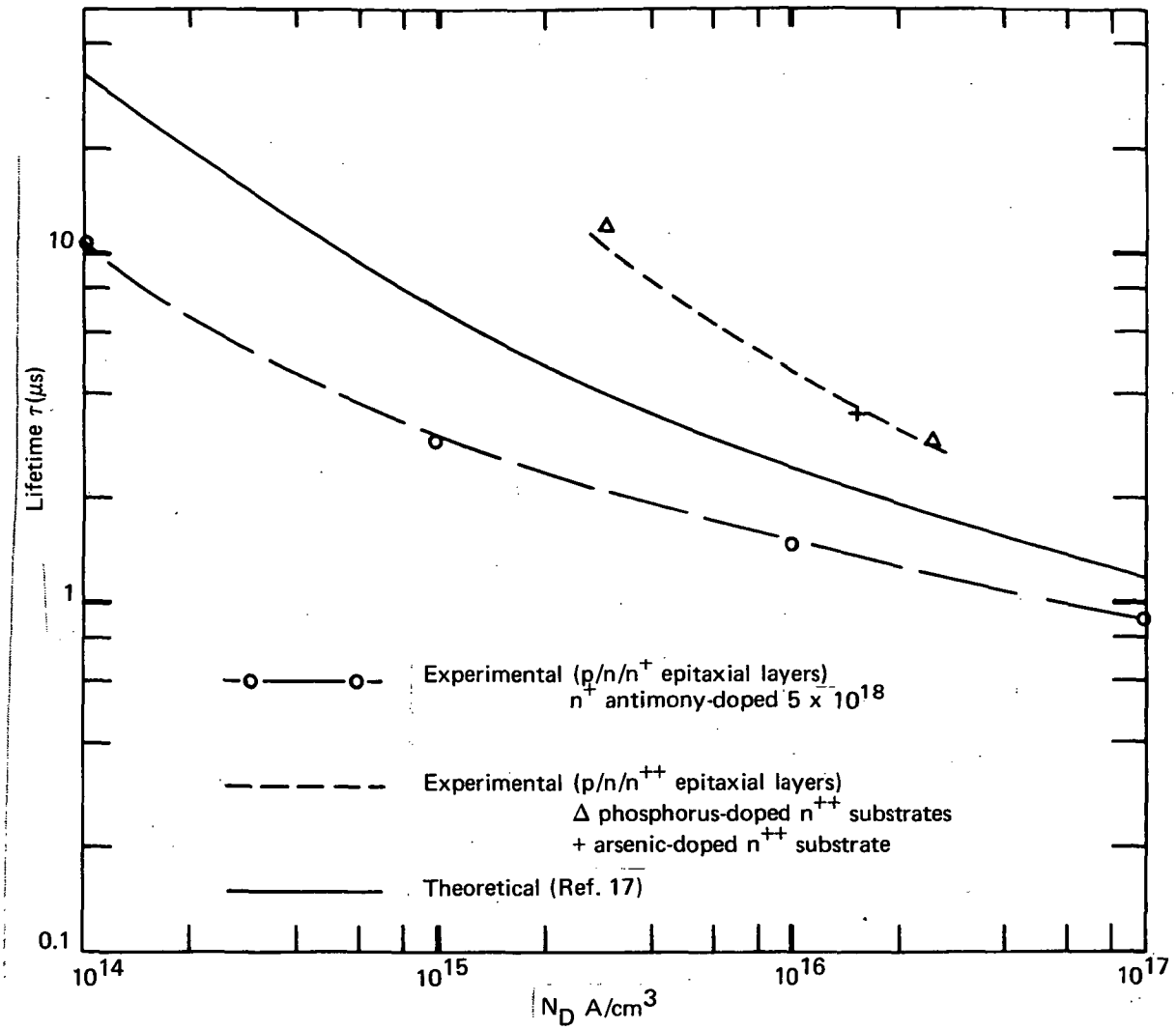

Figure 5. Lifetime as a function of doping level for p/n epitaxial layers.

The I-V characteristics of the device under test (DUT) were measured using the circuit shown in Fig. 6, and the data were plotted on a semi-logarithmic scale in order to determine the parameters which characterize the p/n and n/p junctions.

The data were analyzed by assuming a diode current of the form

$$J_T(v) = \underbrace{J_{01} \exp\,[qV/n_2kT-1]}_{J_2} + J_o \exp[qV/nkT-1] \qquad (6)$$

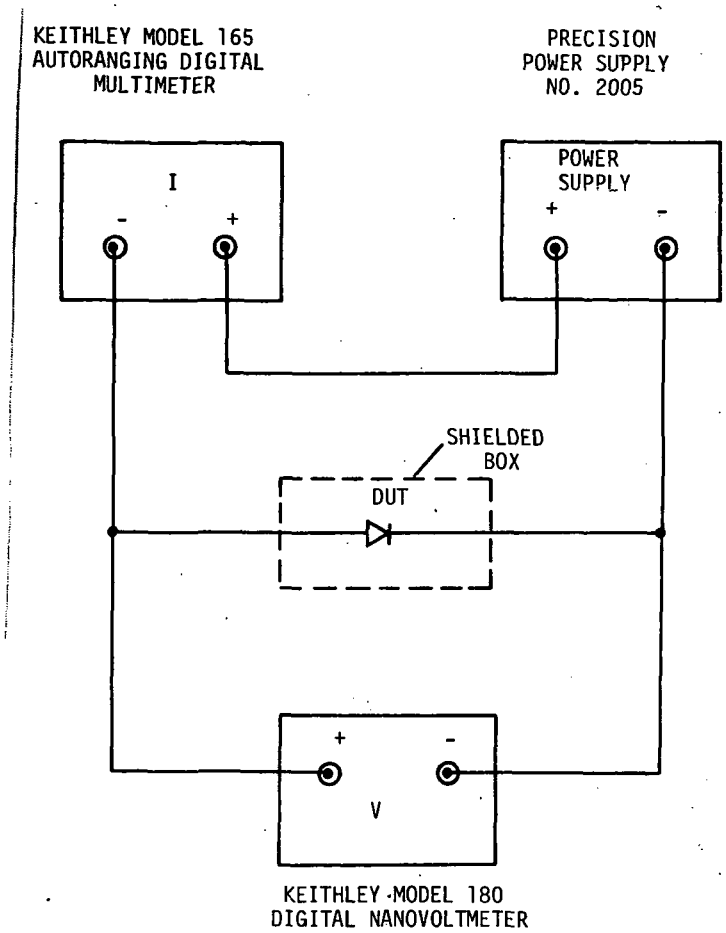

Figure 6. Circuit for diode I-V measurement.

J_o and n were obtained by plotting $\ell n\ [J_T - J_2]$ versus voltage, and extracting the slope and intercept.*

1. $p/n/n^+$ and $p/n/n^{++}$ Structures. - Measured I-V curves for p/n junctions grown on 5×10^{18} A/cm^3 n^+ antimony-doped substrates are shown in Figs. 7 and 8. Figure 9 shows similar data for $p/n/n^{++}$ layers grown on 1×10^{20} n^{++} phosphorus-doped substrates. The junction n factors and J_o saturation currents are given in each figure. The data indicate that the epitaxial junctions have good I-V characteristics and that the junctions grown on n^{++} phosphorus substrates are somewhat better than the junction layers grown on n^+ antimony-doped substrates.

*This method was suggested by H. W. Brandhorst of NASA-Lewis Research Center, Cleveland, Ohio.

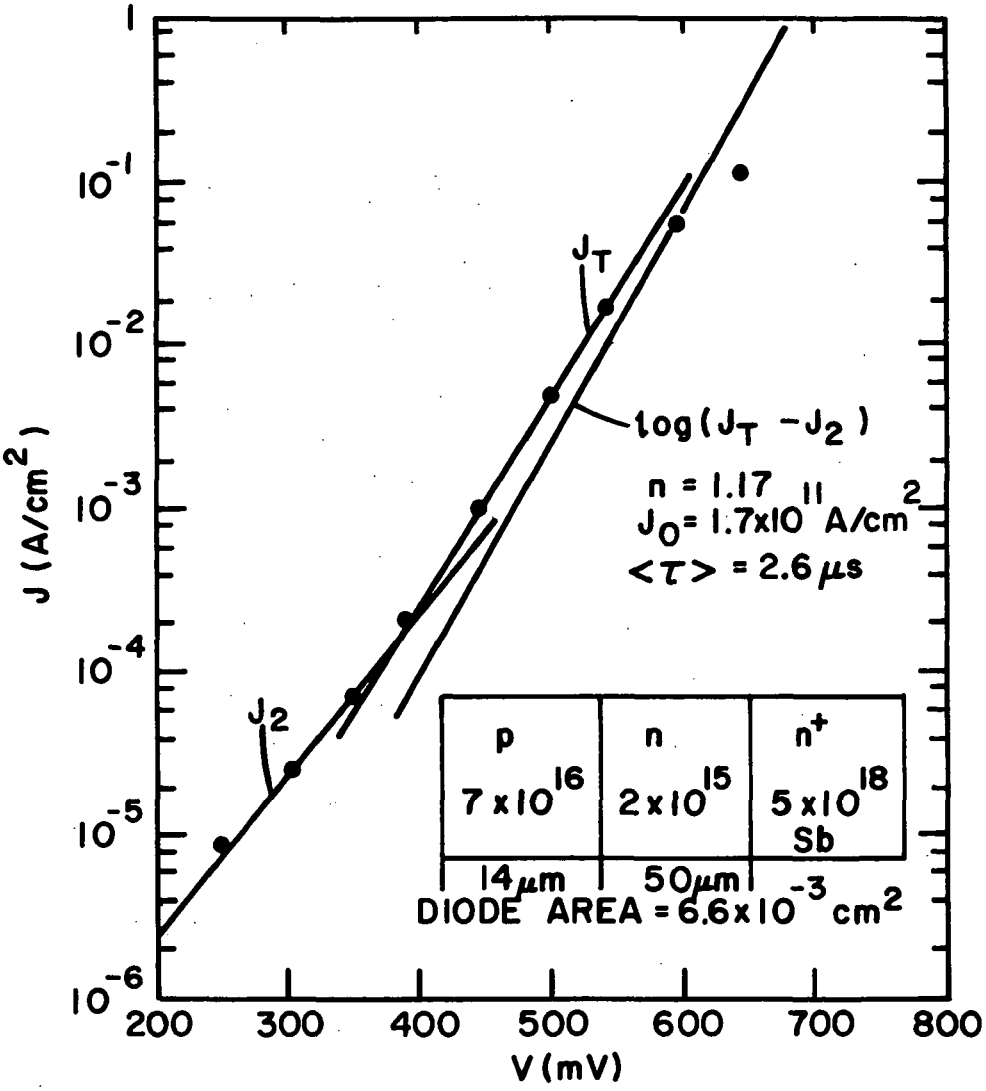

Figure 7. I-V characteristics and parameters for a p/n epitaxial junction on n^+ antimony-doped substrate.

Figure 7 I-V characteristics and parameters for a p/n epitaxial junction on n+ antimony-doped substrate.

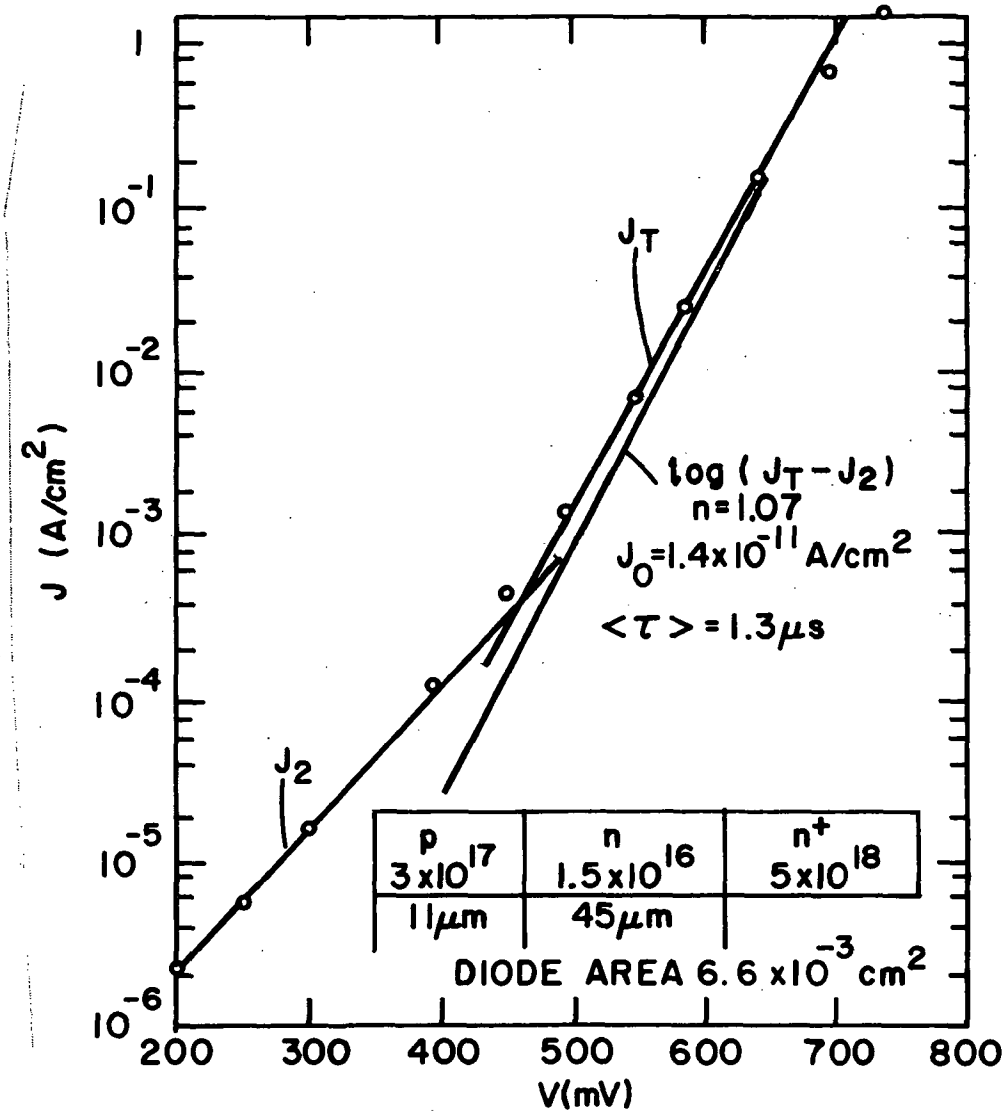

Figure 8. I-V characteristics and parameters for a p/n epitaxial junction on n^+ antimony-doped substrate.

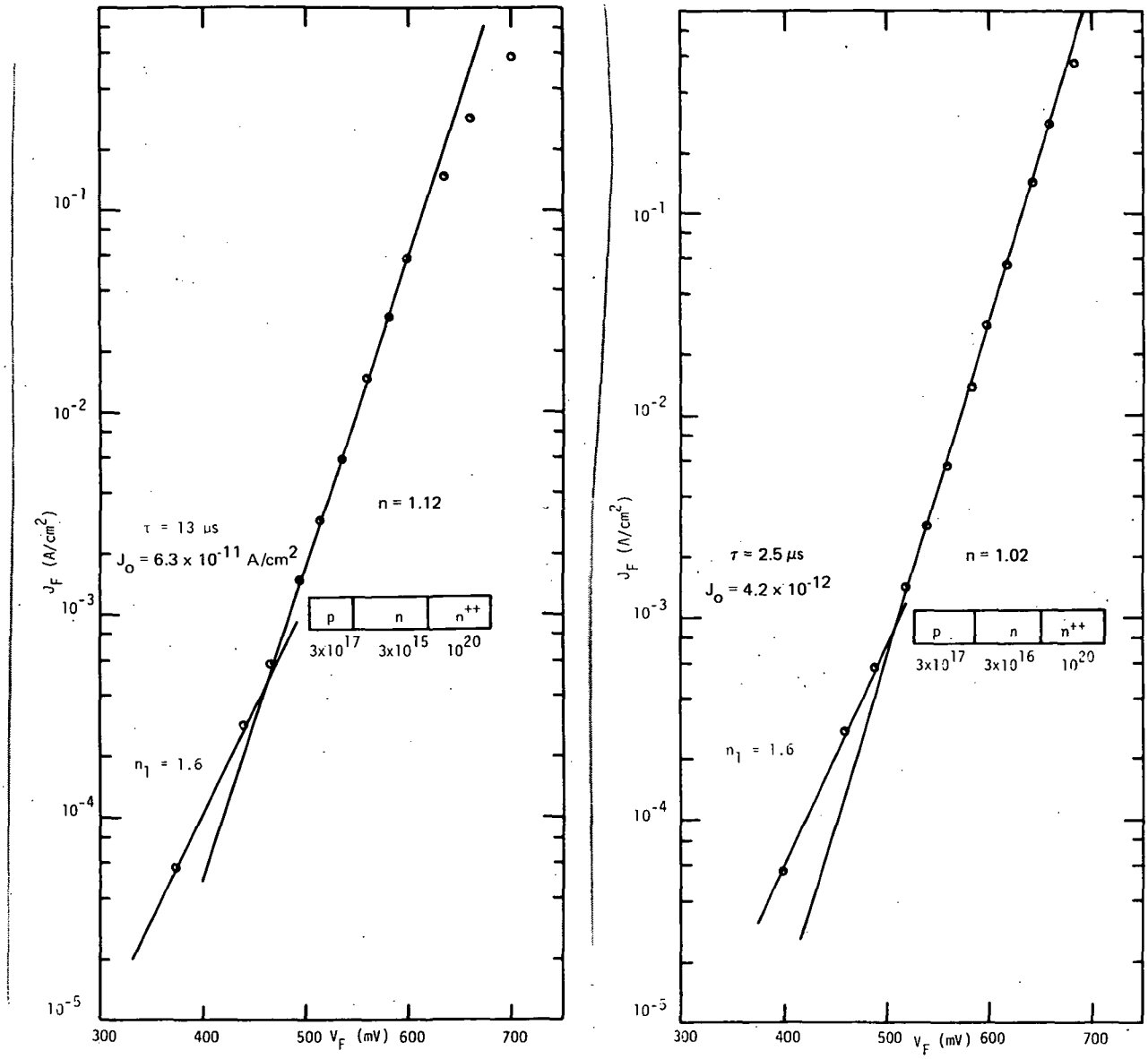

Figure 9. I-V characteristics for a p/n epitaxial junction on n^{++} phosphorus-doped substrate.

2. n/p/p^+ Structures. - Similar data are presented for diodes in Figs. 10, 11, and 12 for the complementary n/p junction layers grown on boron-doped p^+ substrates. Equally good I-V characteristics are obtained for this case.

It should be noted that the recombination-related current density generally increases for the higher doped p-base structures having the lower lifetimes.

The variation of measured lifetime with p-layer acceptor concentration is shown in Fig. 13. The lifetime values and variation with concentration are similar to those for the p/n epitaxial layers in Fig. 5.

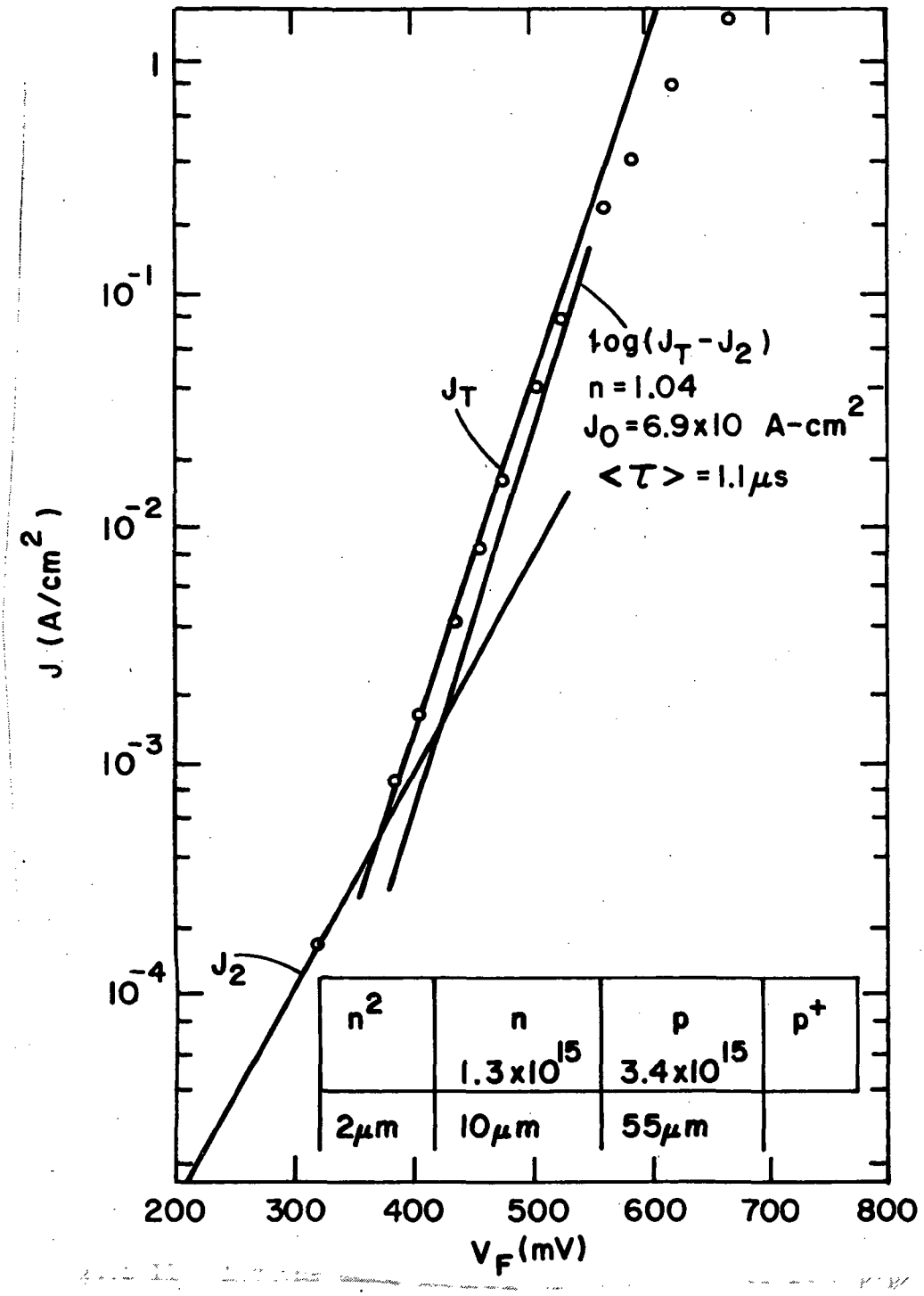

Figure 10. I-V characteristics and parameters for an n/p/p^+ epitaxial structure.

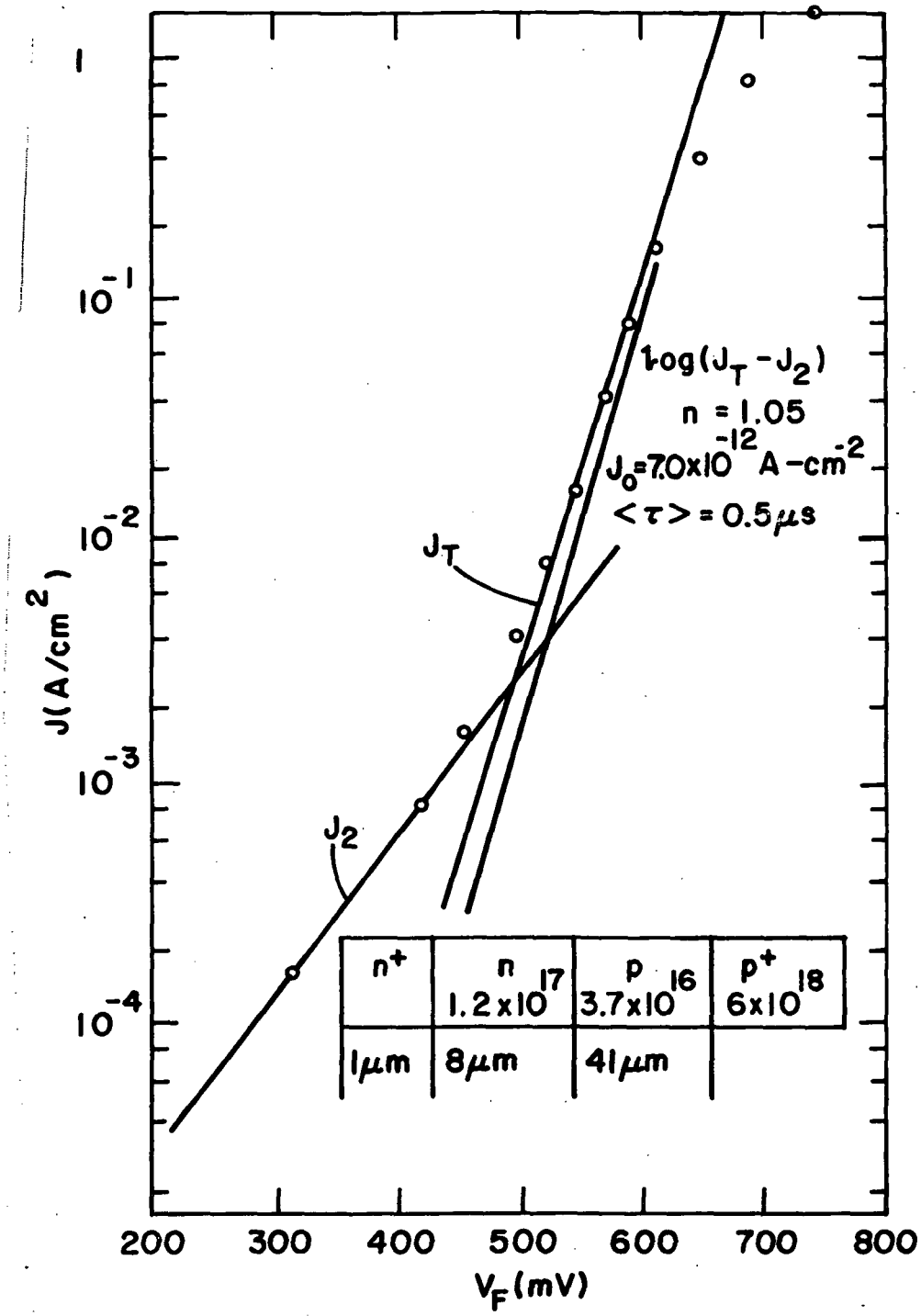

Figure 11. I-V characteristics for a n/p/p$^+$ epitaxial structure.

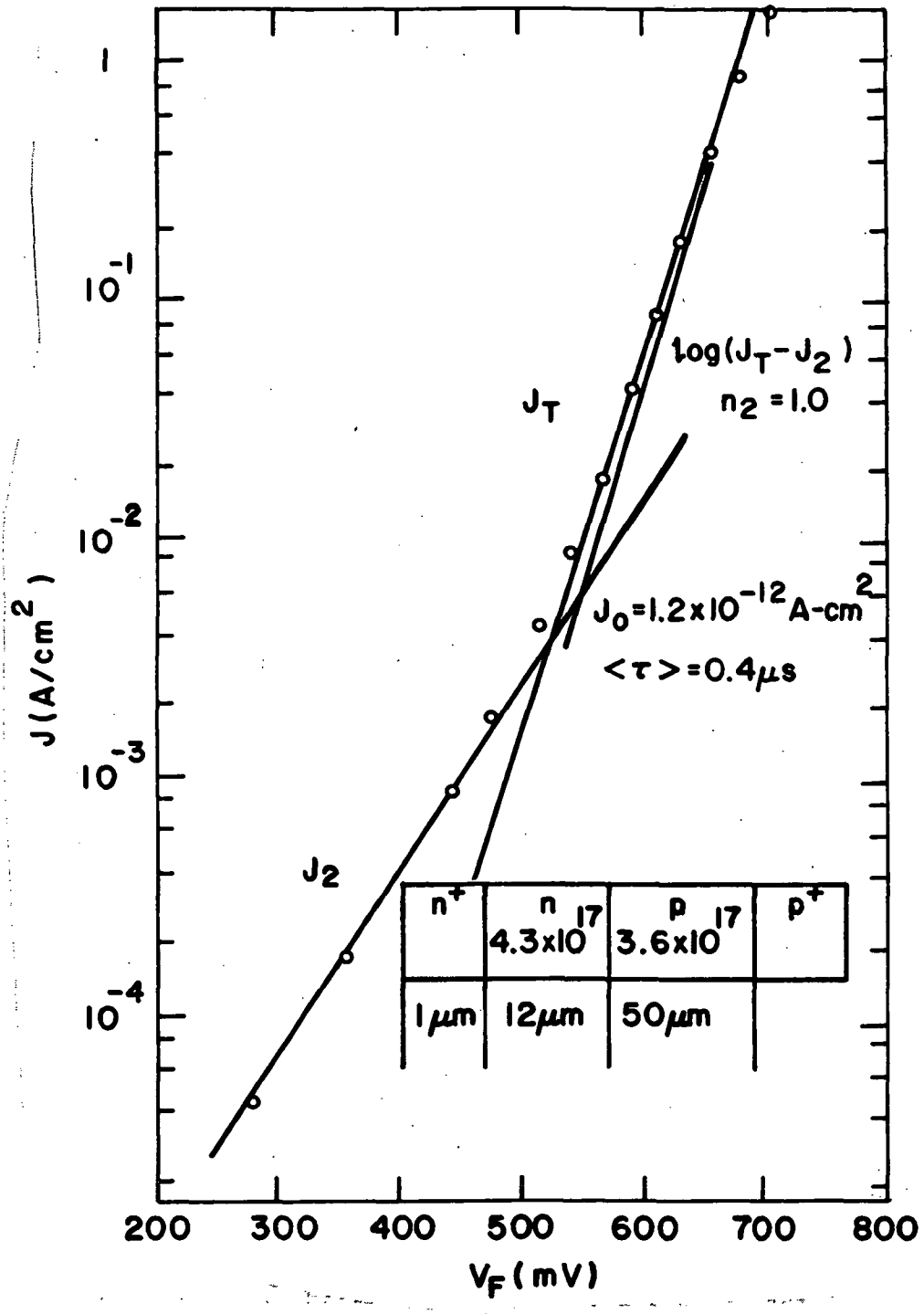

Figure 12. I-V characteristics for a n/p/p^+ epitaxial structure.

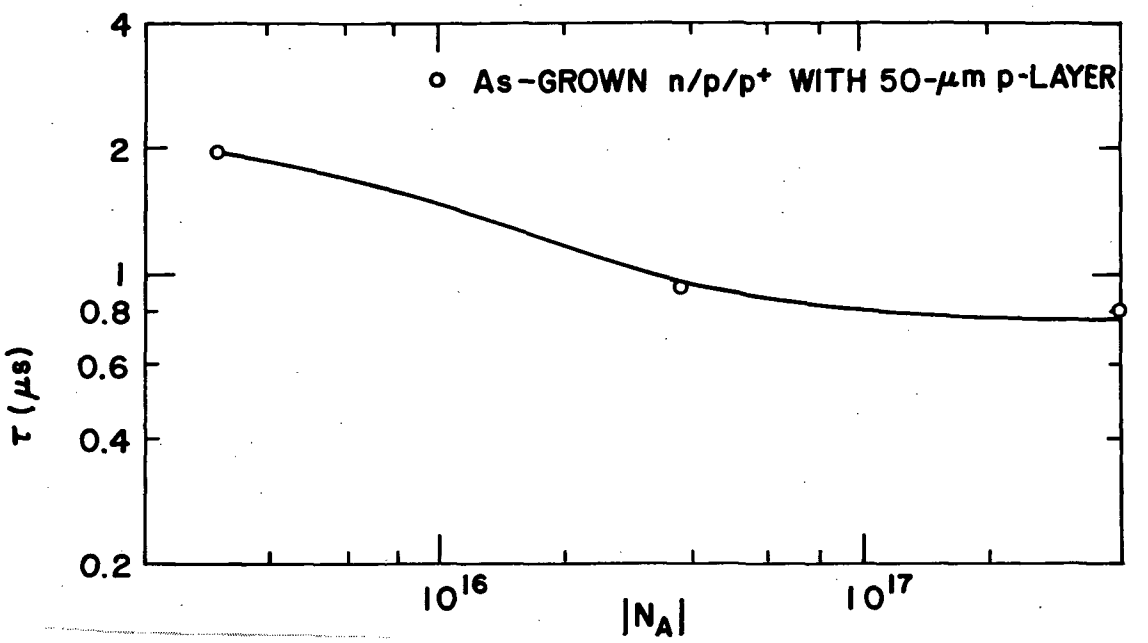

Figure 13. Lifetime of 50-μm p-layer as a function of doping in p-epitaxial base.

V. SOLAR CELL FABRICATION AND PERFORMANCE - $p/n/n^+$ STRUCTURES

Having established the material and junction characteristics in relation to the growth conditions for the epitaxial layers, we fabricated and evaluated solar cells. In this section, solar cell performance for $p/n/n^+$ structures grown using dichlorosilane is described and related to the epitaxial cell structure and to the junction I-V characteristics.

Cells having an epitaxial $p/n/n^+$ structure were studied having either a uniformly doped n-base or an intentionally graded n-base layer. The effect of adding a p^+ diffusion to the surface layer resulting in a $p^+/p/n/n^+$ structure is described.

A. Cell Fabrication and Measurements

The fabrication procedures described here apply only to the epitaxial $p/n/n^+$ structures.

After the epitaxial layers were grown, the layers were characterized for thickness and doping density profile by spreading resistance techniques. Wafers were then processed into solar cells and diagnostic diodes by the following processing steps:

(1) Clean wafers in (a) H_2O_2/H_2SO_4 (1:1) solution, (b) $H_2O/H_2O_2/NH_3OH$ (4:1:1), boiling for 10 min, (c) $H_2O/H_2O_2/HCl$ (5:1:1), boiling for 10 min. (Rinse in filtered DI water between each cleaning step.)
(2) Diffuse p^+ using boron-doped oxide, deposited at 370°C from silane, followed by 925°C drive-in for 2 h. Slow cool to 675°C at 2°C/min. Open tube furnace with argon flowing.*
(3) Strip oxides; clean.
(4) Evaporate Cr/Au, ∿200 Å/4000 Å, through metal mask, forming top finger contact.
(5) Evaporate Cr/Ni, 300 Å/1 μm, back contact.

*In initial experiments, this step was not used; instead, a thermal oxide was grown at 900°C for 20 min. The oxide serves as the AR coating and surface passivant. This was followed by a photoresist step to open contact areas for metallization. The metal pattern was later defined by an additional photoresist step. A comparison of cells fabricated on similar epitaxial structures by both procedures is given in Section V-C.

(6) Evaporate 700 Å, Al_2O_3 AR coating.*
(7) Mesa etch to a depth of 0.00504 cm (2 mils) to define junction.

A photomicrograph of one-half of a completed wafer containing one cell and six diagnostic diodes is shown in Fig. 14. The cell contact geometry is shown in schematic detail in Fig. 15. For this geometry, it can be shown (ref. 3) that if the surface layer sheet resistance is $R_\square$ Ω/□, then the portion of the series resistance of the cell contributed by the top layer is given by

$$R_s = \frac{R_\square}{8} \times \frac{\ell}{w} \times \frac{1}{(n-1)^2} \tag{7}$$

where ℓ is the length and w the width, and n is the number of fingers. For a typical value of $R_\square = 100$ Ω/□, $R_s = 0.28$ Ω.

The area coverage for this pattern is 14%, a value not optimized for minimum area coverage.

Spectral response curves and illuminated I-V characteristics for the solar cells were measured using an AM-1 simulator described in Appendix B. Solar cell performance was also measured under New Jersey sunlight conditions. In all cases, the radiation intensity was measured using calibrated solar cells provided by NASA.**

Dark I-V characteristics were measured on cells and diagnostic diodes by conventional four-point techniques. The lifetimes were obtained from measurements of open-circuit voltage and reverse recovery methods as described in Appendix A.

B. $p/n/n^+$ Epitaxial Cells

Initial experiments were conducted on $p/n/n^+$ epitaxial cells with no p^+ diffusion into the surface layer. To evaluate the effects of the doping profile, three cell profiles were grown having nominally the same layer thickness, but different doping density profiles in the p- and n-layers. These structures are shown in Figs. 16, 17, and 18. The first (Fig. 16) contains an approximate exponential gradient in the n-base, and the second (Fig. 17) has a uniform n-base with a gradient only in the p-surface layer. The third structure (Fig. 18) is uniformly

*This step is omitted if a thermal oxide is used in step 2.
**Cells and calibration data provided by H. Brandhorst and C. Swartz of NASA-Lewis Research Center, Cleveland, Ohio.

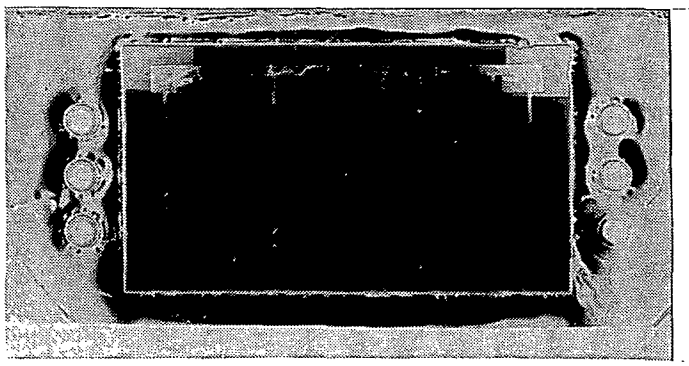

Figure 14. Photomicrograph of solar cell and diagnostic diodes.

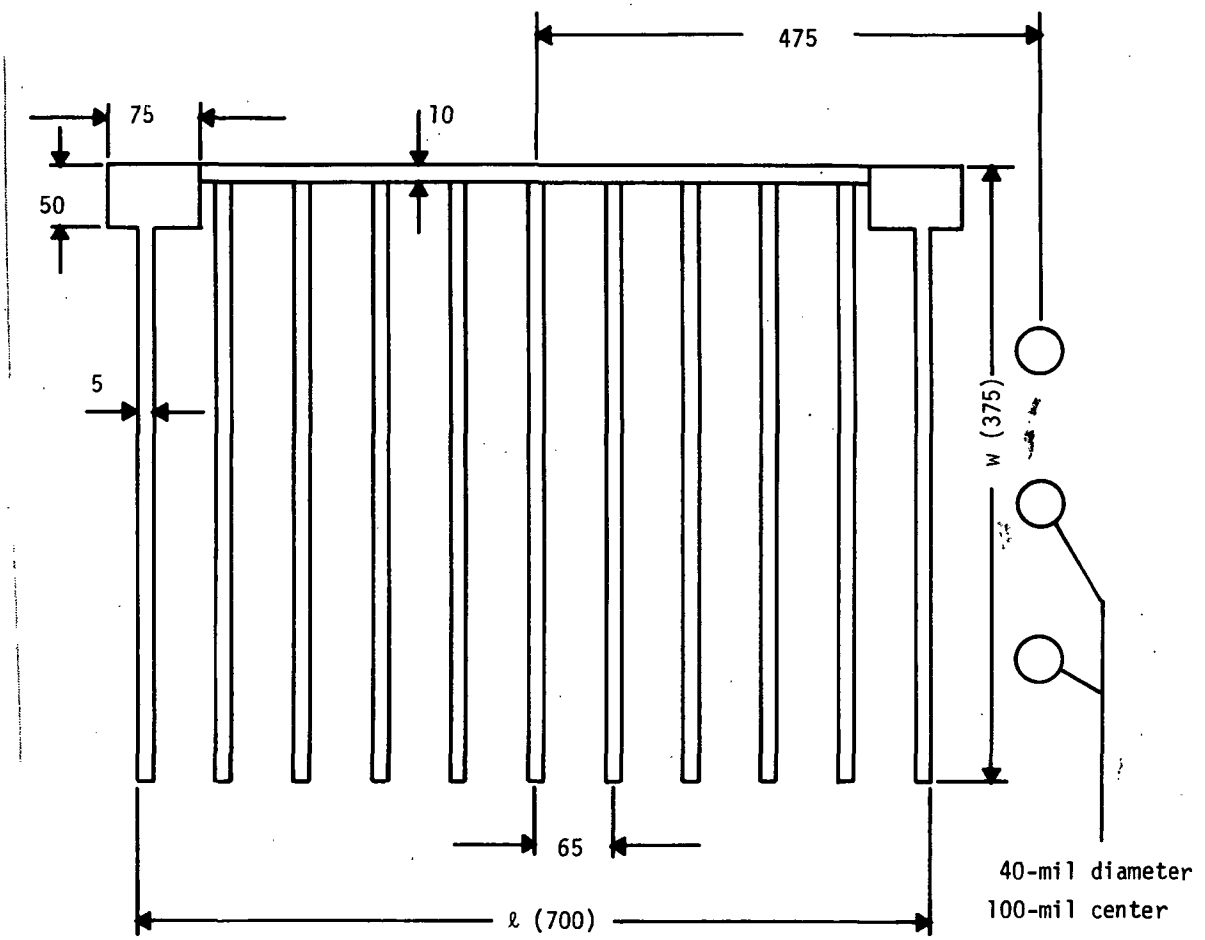

NOT TO SCALE; ALL DIMENSIONS IN MILS.

Figure 15. Horizontal metallization geometry used in solar cell fabrication.

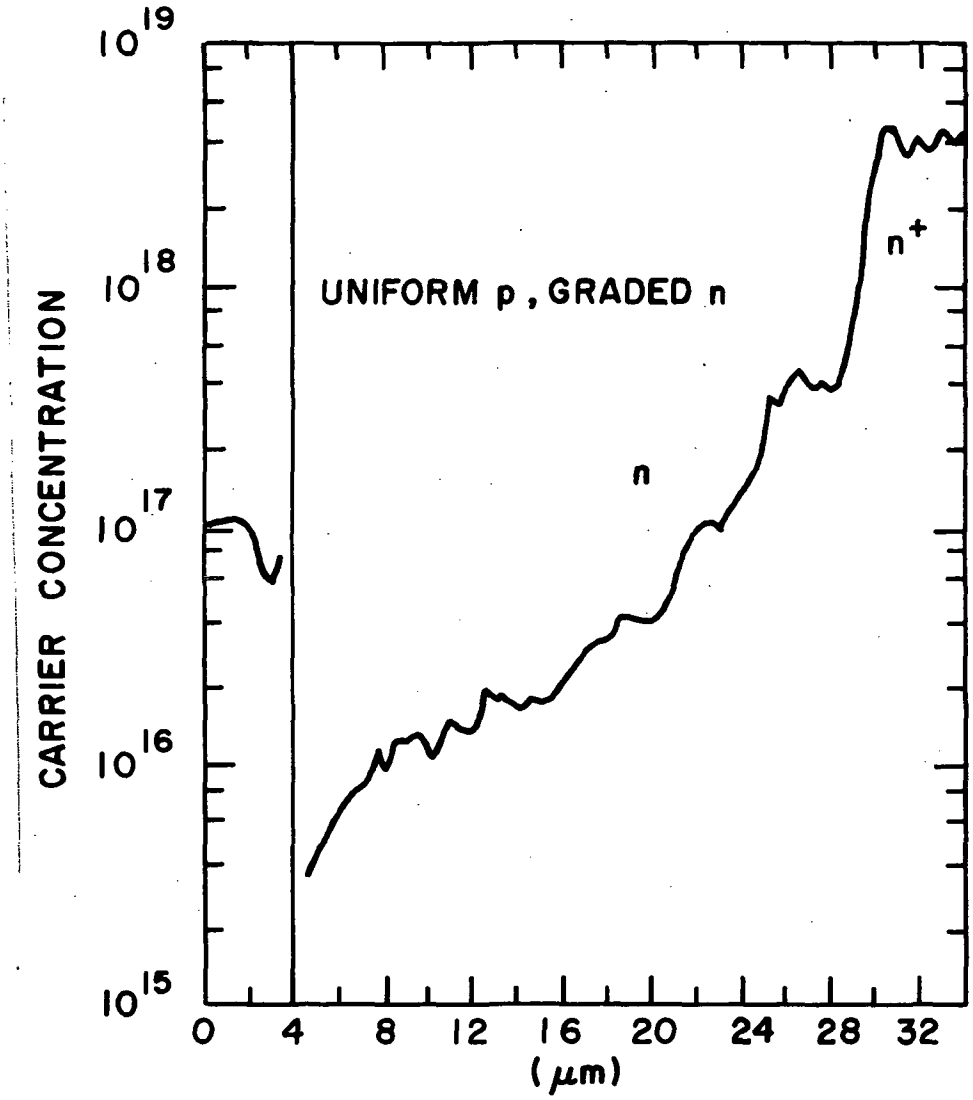

Figure 16. Doping profile of an epitaxial, uniform p, graded n solar cell structure (#664204). (Same as Fig. 4; repeated here for the convenience of the reader.)

doped on both sides of the junction. These profiles were achieved by control of the dopant gas flow during epitaxial growth.

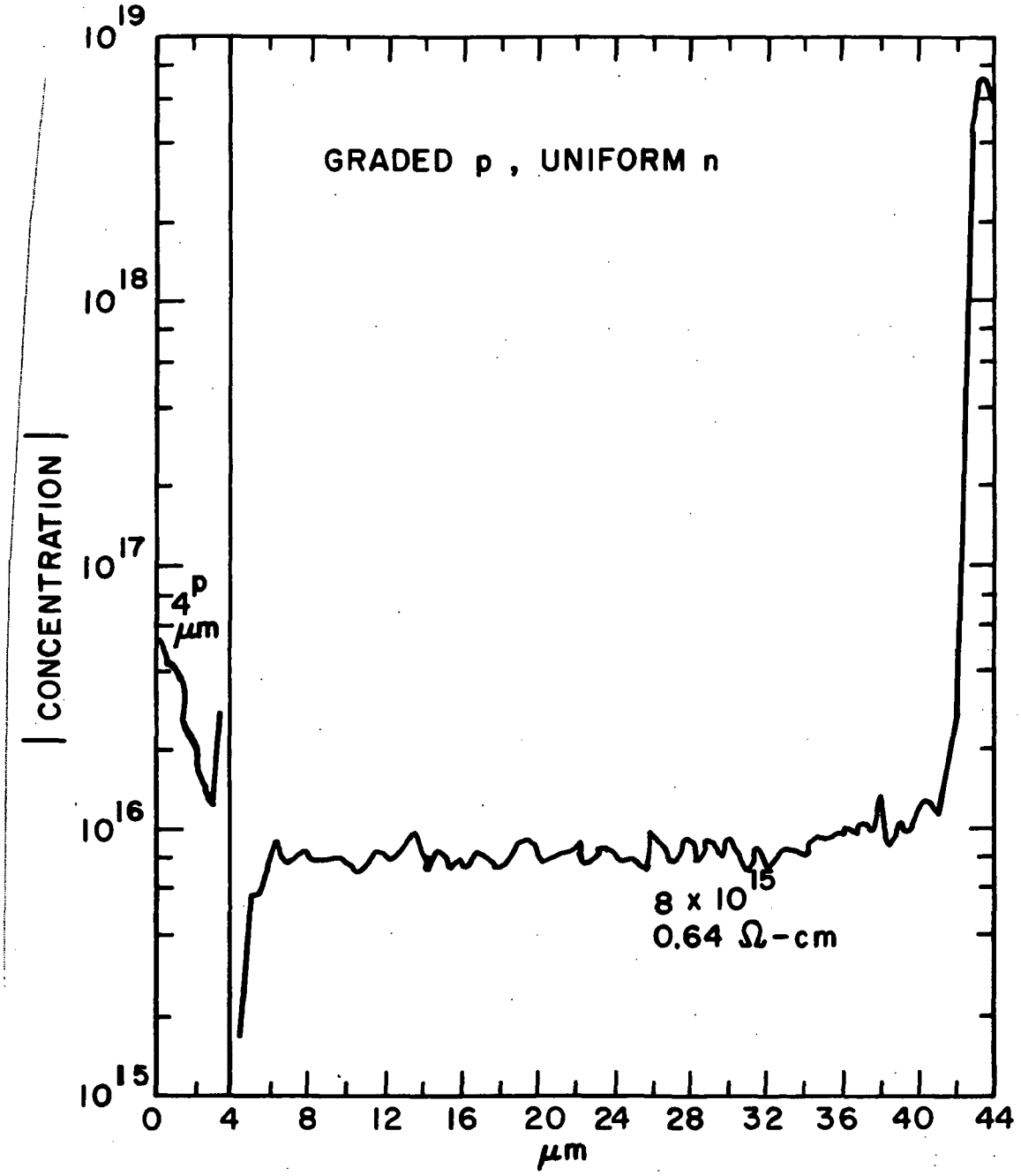

Figure 17. Doping profile of an epitaxial, graded p, uniform n solar cell structure (#665996)

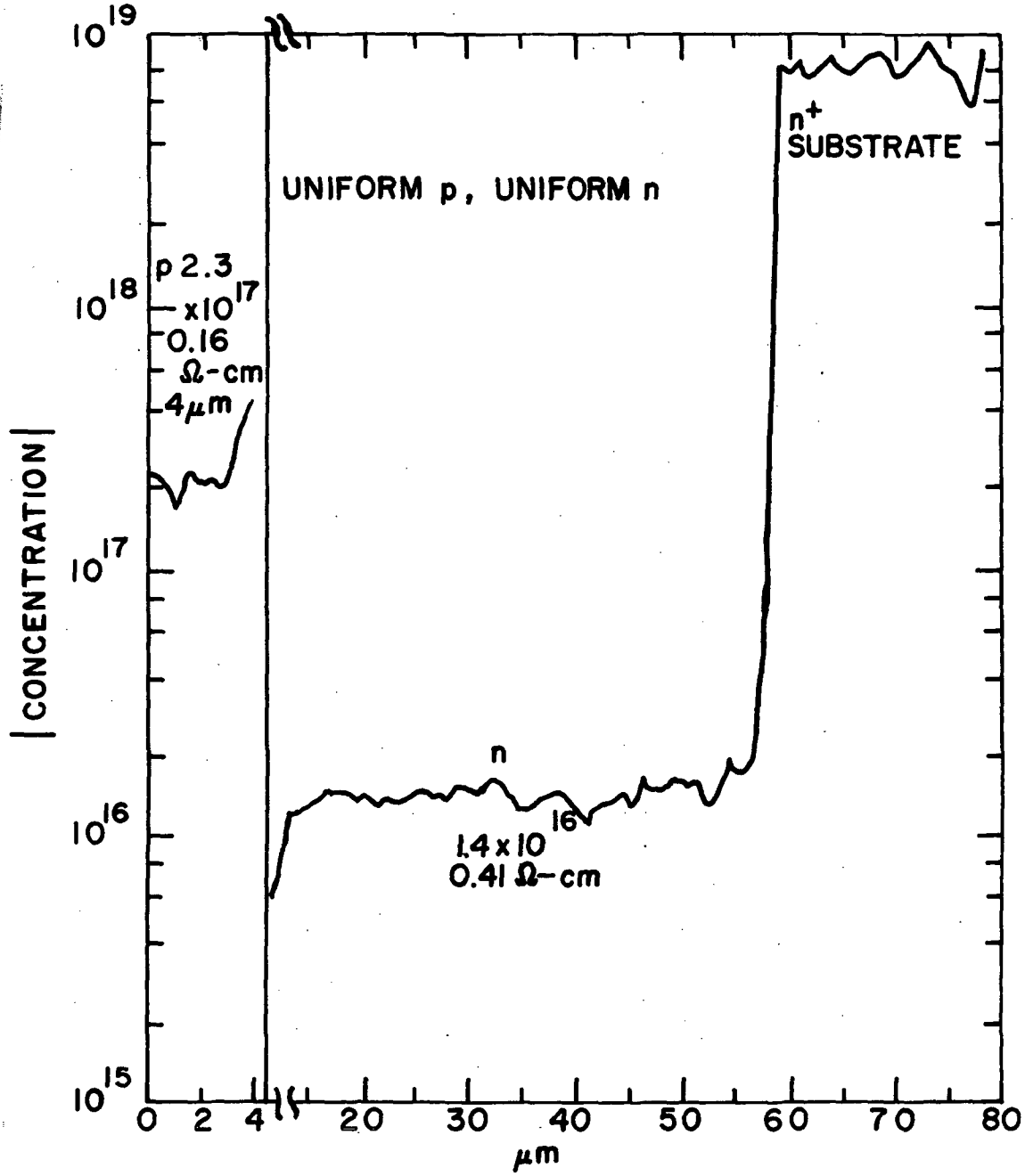

Figure 18. Doping profile of an epitaxial, uniform p, uniform n solar cell structure (#573360)

The important cell parameters are summarized in Table III, and the illuminated I-V curves are given in Figs. 19, 20, and 21. Spectral response curves are shown in Fig. 22.

TABLE III. SOLAR PARAMETERS FOR THREE EPITAXIAL CELL STRUCTURES

	J_{sc} I_{SC_2} (mA/cm^2)	V_{oc} (mV)	F.F.	P_{max} (mW/cm^2)	η (%)	Solar or Lamp Intensity (mW/cm^2)
Cell #664204 Uniform p/graded n						
Sun	24.1	589	0.78	11.0	11.1	99
AM-1	23.5	588	0.78	10.9	11.0	94
AM-0(a)	26.7	592	0.79	12.5	9.3	135.3
Cell #665996 Graded p/uniform n						
Sun	22.8	572	0.75	9.8	10.1	97
AM-1	22.9	576	0.78	10.3	10.3	100
AM-0(a)	25.4	578	0.79	11.6	8.6	135.3
Cell #573360 Uniform p/uniform n						
Sun	16.4	579	0.77	7.3	7.4	98
AM-1	16.8	584	0.78	7.7	7.7	100
AM-0(a)	19.1	588	0.78	8.8	6.5	135.3

(a) Measured at NASA-Lewis with AM-0 simulator.

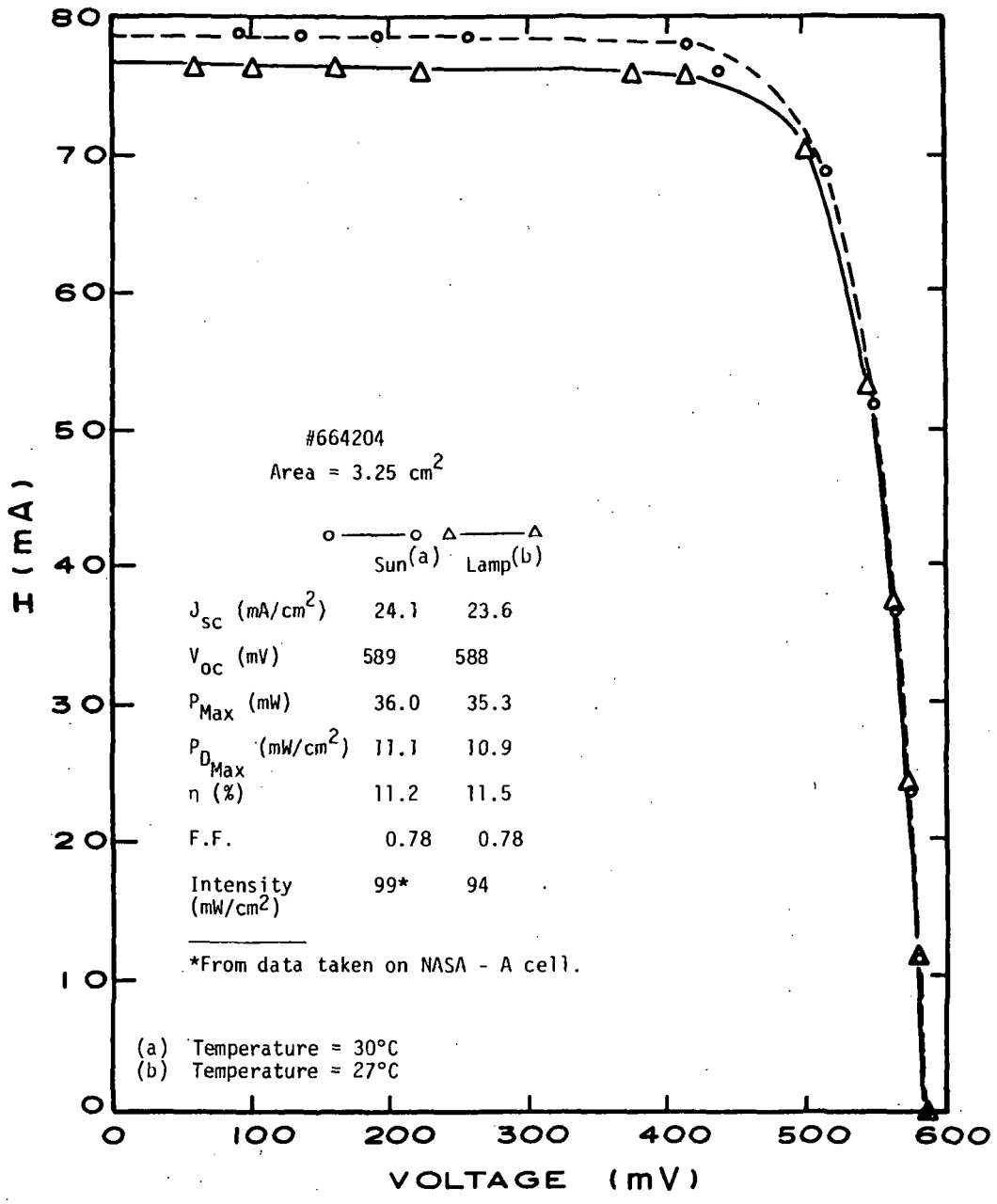

Figure 19. Illuminated I-V characteristics for epitaxial cell #664204 obtained in sunlight and with AM-1 solar simulator.

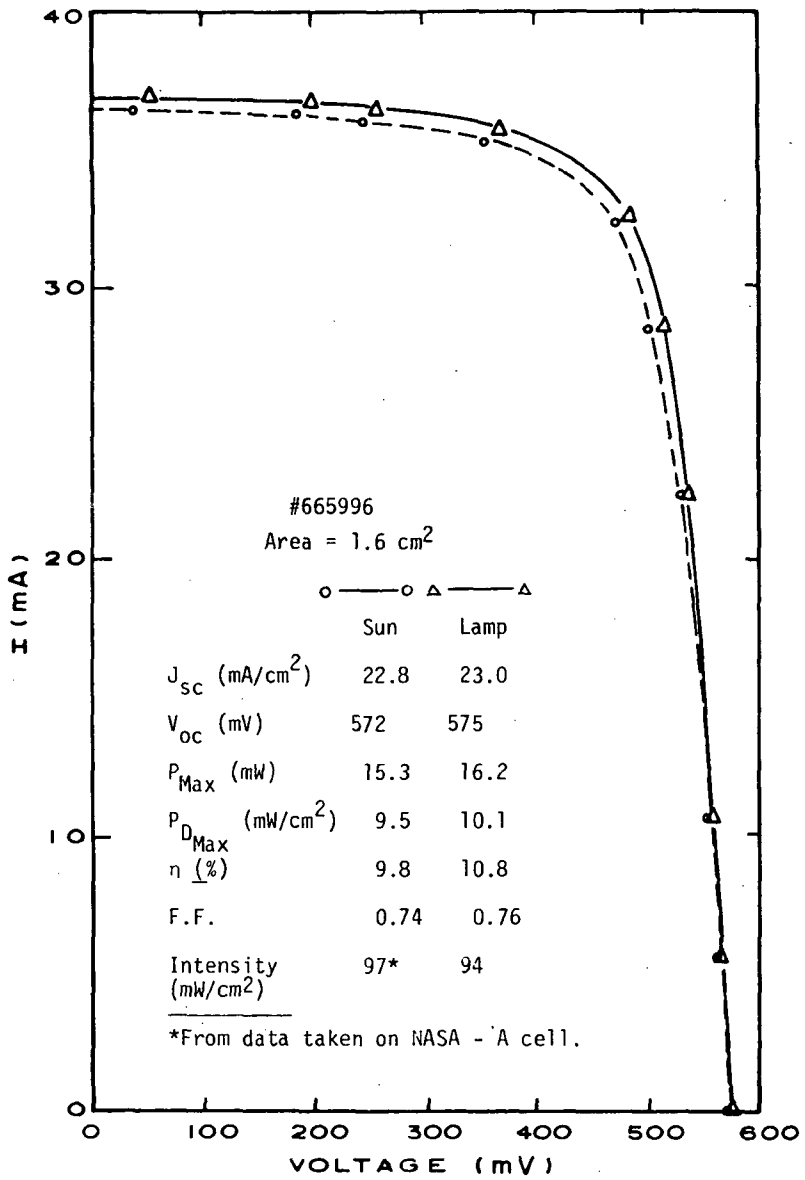

Figure 20. Illuminated I-V characteristics for epitaxial cell #665996 obtained in sunlight and with AM-1 solar simulator

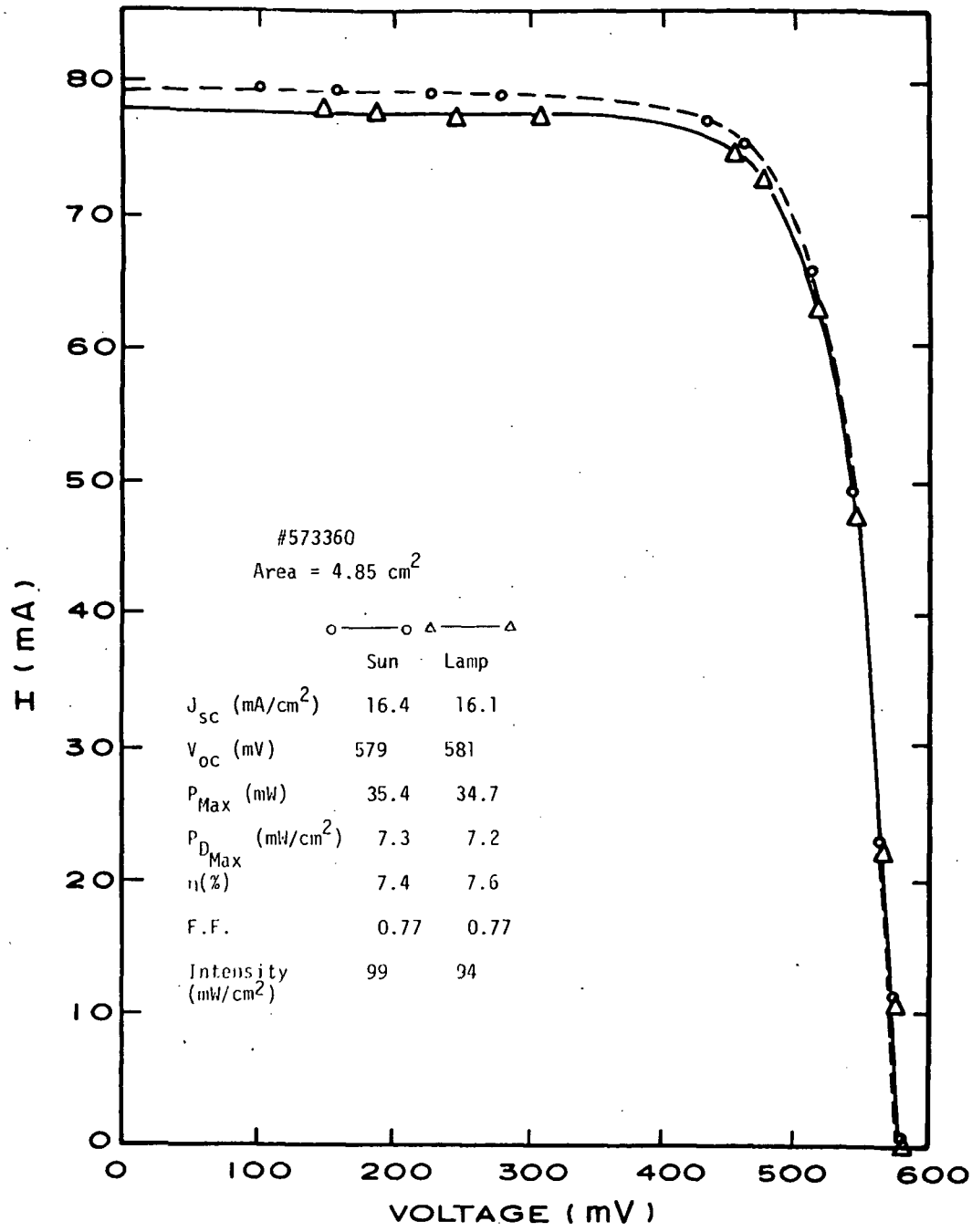

Figure 21. Illuminated I-V characteristics for epitaxial cell #573360 obtained in sunlight and with AM-1 solar simulator

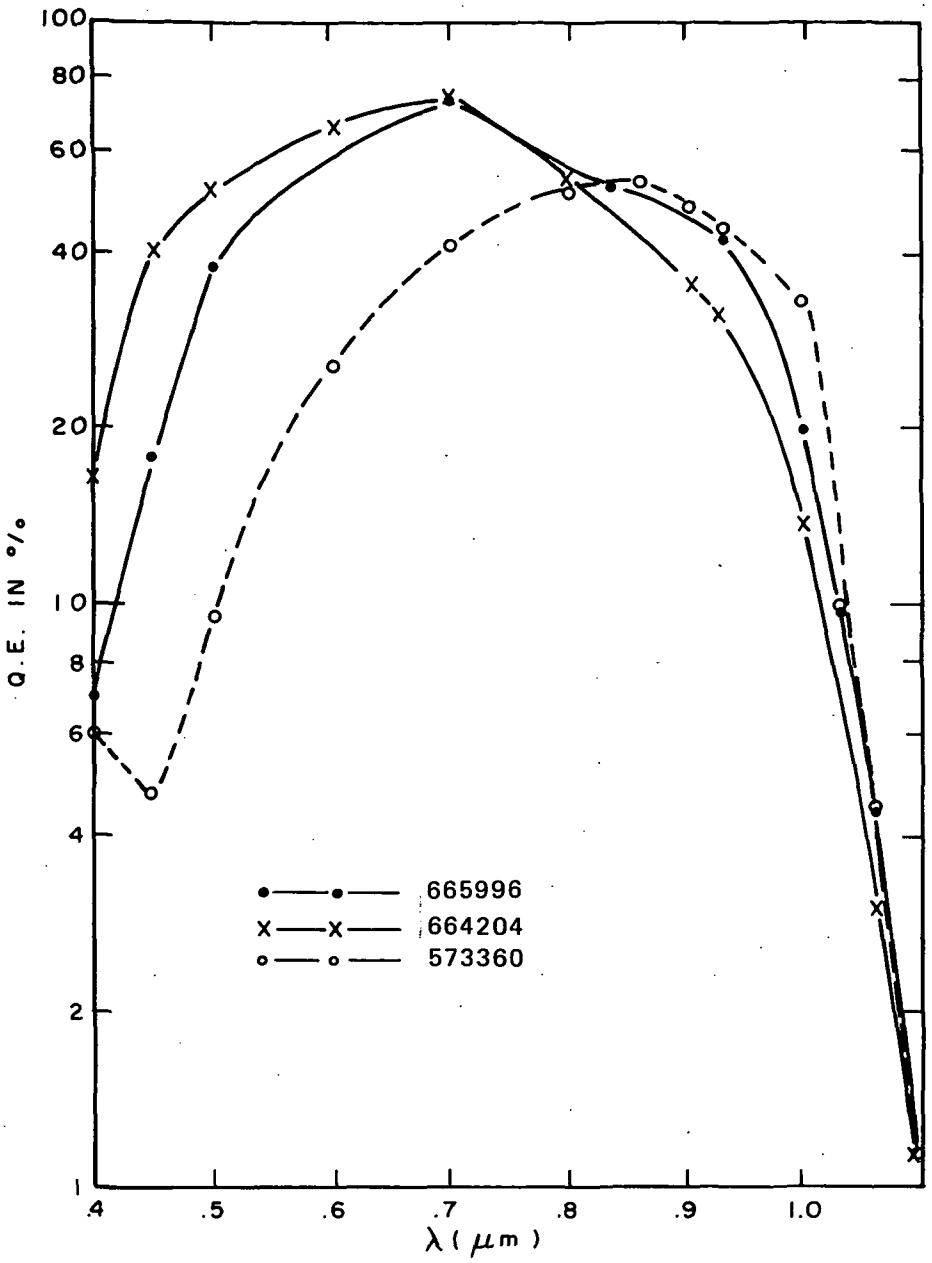

Figure 22. Spectral response curves for cell #664204, #665996 and #573360.

From these data, several tentative conclusions were drawn which indicated a direction for improvement in cell performance described later in Section C. These are:

(1) Cells with graded profiles outperformed uniformly doped cells.
(2) The cell with a graded n-base has the best overall parameters and spectral response.
(3) High open-circuit voltages result from these structures. Highest V_{oc} is obtained for the structure with graded n-base.
(4) All cell structures suffer from poor blue response. In particular, the cell with a uniform p-surface layer has the poorest low wavelength response.
(5) Good fill-factors and high open-circuit voltages indicate good junction quality.

As a consequence of these observations, it was decided to study graded structures in more detail. The poor blue response indicates that improvements are needed in the surface layer. For this reason, narrower p-layers were grown and a p^+ surface diffused layer was incorporated in later structures. The p^+ diffused region provides a drift field which aids the motion of electrons toward the p/n junction (ref 18). In principle, this gradient can be obtained by epitaxial methods; however, the particular gas system and reactor combination used in our laboratory was limited to surface concentration of less than 10^{18} A/cm^3.

The use of epitaxial techniques to grow the n-base and p-layer, combined with a p^+ diffusion allows for the study of $p^+/p/n/n^+$ structures containing a graded-base (refs. 19, 20) and a graded surface layer. Such a structure is described in the next section.

C. $p^+/p/n/n^{++}$ Graded Base Structures

To more fully evaluate epitaxial graded-base solar cells, two epitaxial structures were grown and studied in detail.

The resulting profiles for these two structures obtained from spreading resistance measurements are shown in Figs. 23(a) and (b). In the insets of these figures, the dashed curves representing the p^+ diffusions are approximate representations, as the spreading resistance technique is subject to great errors for very shallow diffusions (ref. 21). The p^+ diffusion and cell fabrication were done by the method described in Section V-A. The resulting measured four-point sheet resistance of the p^+ diffusion was 85 Ω/□. Our experience, and other measurements, indicate that the surface concentration of this p^+ layer is $\lesssim 7 \times 10^{19}$ A/cm^3.

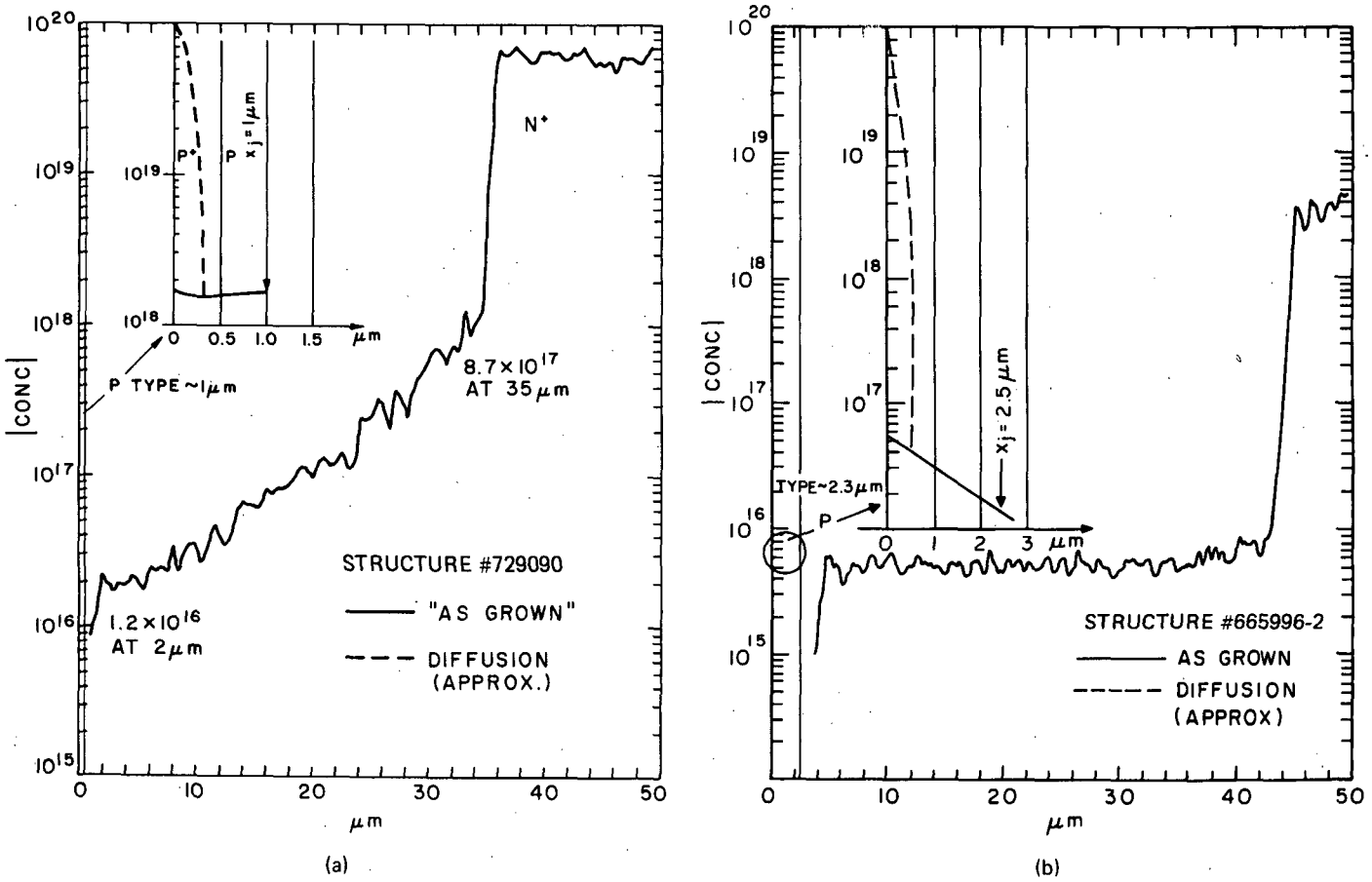

Figure 23. Concentration profiles of two epitaxial solar cell structures: (a) graded n-base and (b) uniform n-base.

For additional comparison, a 1-Ω-cm bulk silicon wafer was simultaneously diffused and processed along with the epitaxial wafer. No back contact diffusion was performed on this sample, resulting in a p^+/n solar cell.

Current-voltage characteristics were measured both in New Jersey sunlight and under the solar simulator lamp. The results of these measurements for the epitaxial and diffused cells are shown in Figs. 24(a) and (b) and 25, and a summary of the solar cell parameters is given in Table IV. The spectral response curves shown in Fig. 26 show that a better blue response is obtained for these cells than for the previous ones, not containing a p^+ diffusion.

Several points should be considered when comparing these data with other solar cells. First, the top metal area coverage is ∿14%, which is a relatively large value as most high-efficiency cells are made with less than 10% metal coverage. These epitaxial cells did not suffer from excessive series resistance (the total measured series resistance was ∿0.2 Ω), indicating that the metal coverage can be reduced. Secondly, the peak quantum efficiency for epitaxial cell #729090 is only 78%, a value limited partially by the Al_2O_3 antireflection coating. The reflection coefficient of the 700-Å Al_2O_3 coating as a function of wavelength is shown in Fig. 27. The data were obtained on a Cary Model #14 spectrophotometer operating in the reflection mode and using an aluminum mirror for reference. The reflection coefficient at the $\lambda/4$ minimum of 9% is considerably higher than that obtained with more optimum coatings such as Ta_2O_5.

D. Evaluation of Epitaxial Cell Performance

The epitaxial cells performed well in most cell parameters, with record-high open-circuit voltage obtained for the graded base structure. High fill-factors and open-circuit voltage result, for the most part, from the near ideal current-voltage characteristics of the grown epitaxial junctions. This is seen, for example, by the dark I-V curves for the graded n-base structure #729090 and the uniform base cell #665995-2 shown in Figs. 28 and 29. In particular, for the graded base structure, the n factor of 1.03 and J_o of 9×10^{-13} A/cm^2 in the diffusion-limited portion of the I-V curve, are close to the theoretically expected values. As a comparison, the dark I-V curves for the p^+/n solar cell fabricated by diffusion, shown in Fig. 30, have n = 1.31 and $J_o = 6.6 \times 10^{-10}$ A/cm^2.

It should be noted that low-level recombination or shunting currents exist in both the epitaxial and diffused cells. Although this current is lower (compare Figs. 28 and 30 at V_d = 0.3 volt) for the epitaxial cells,

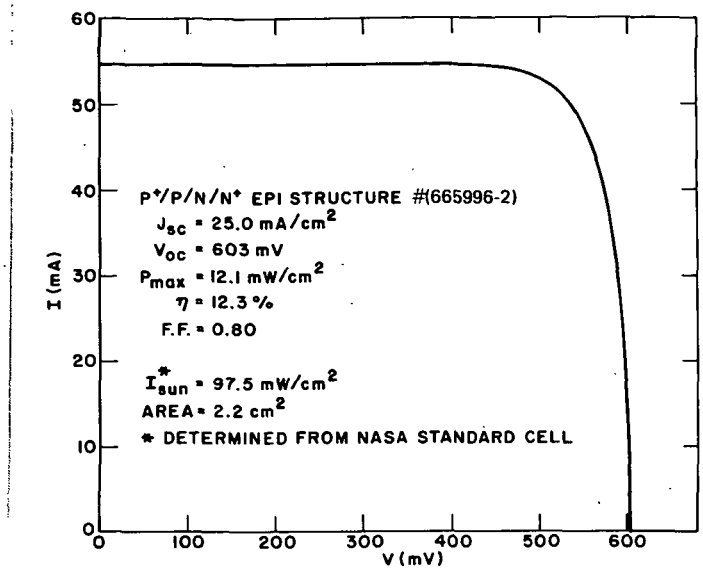

(a)

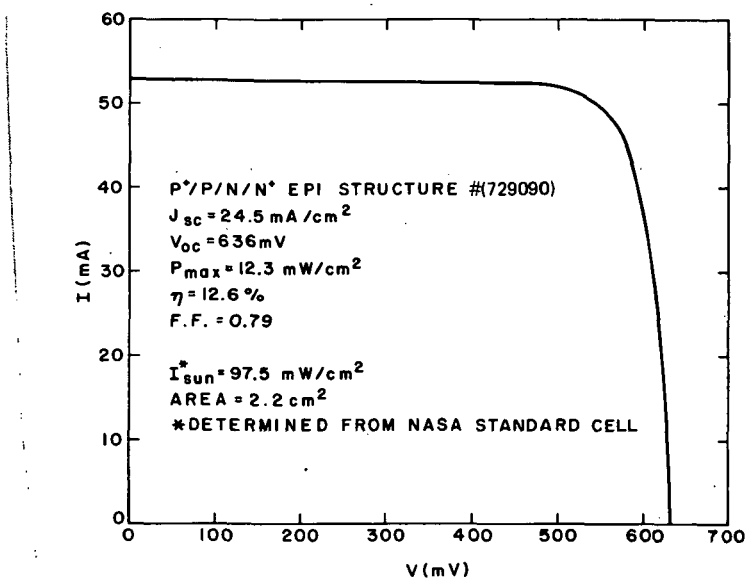

(b)

Figure 24. Illuminated I-V curves for (a) graded base structure #729090 and (b) uniform base structure #665966-2.

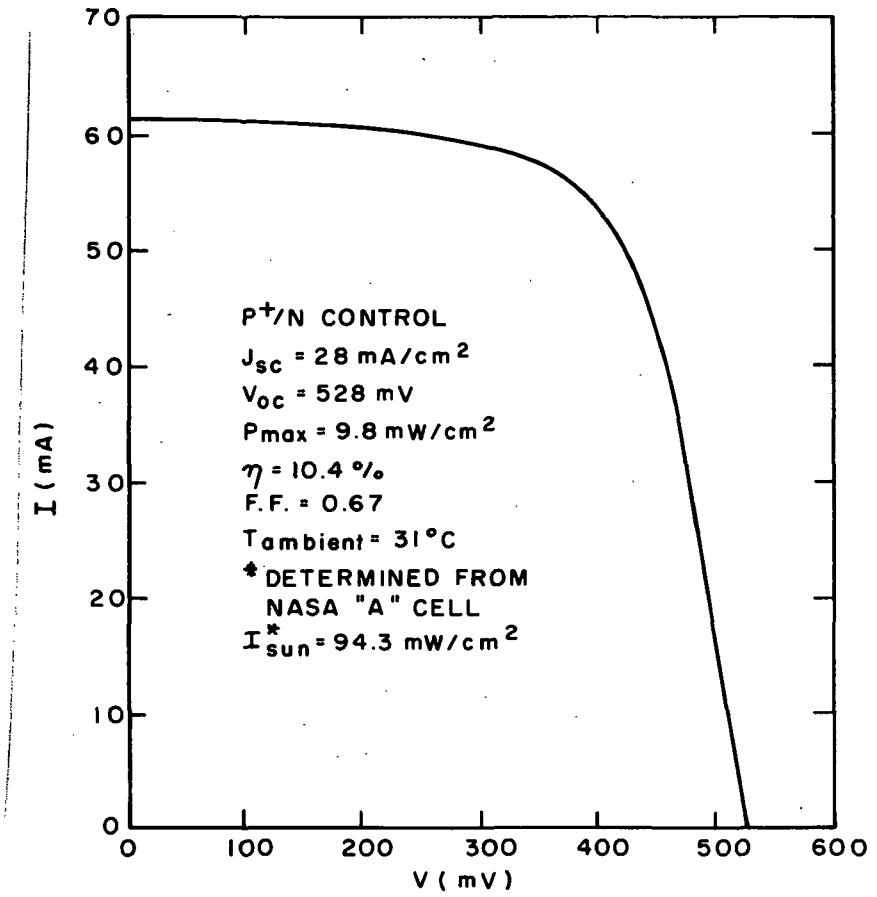

Figure 25. Illuminated I-V curve for diffused p^+/n solar cell.

TABLE IV. SOLAR CELL PARAMETERS FOR TWO EPITAXIAL AND ONE DIFFUSED CELL

	J_{sc} (mA/cm^2)	V_{oc} (mV)	F.F.	P_{max} (mW/cm^2)	η (%)	Solar or Lamp Intensity (mW/cm^2)
Cell #729090 $p^+/p/n/n^{++}$ graded n						
Sun	24.5	636	0.79	12.3	12.5	98
AM-1	25.1	630	0.79	12.5	12.5	100
AM-0(a)	28.3	632	0.79	14.1	10.4	135.3
Cell #665996-2 $p^+/p/n/n^{++}$ uniform n						
Sun	25.0	603	0.80	12.1	12.3	98
AM-1	25.3	606	0.80	12.3	12.3	100
AM-0(a)	28.8	608	0.80	14.1	10.4	135.3
Diffused p^+/n bulk						
Sun	28.9	530	0.67	10.4	10.6	98
AM-1	29.9	532	0.68	10.8	10.8	100

(a) Measured at NASA-Lewis.

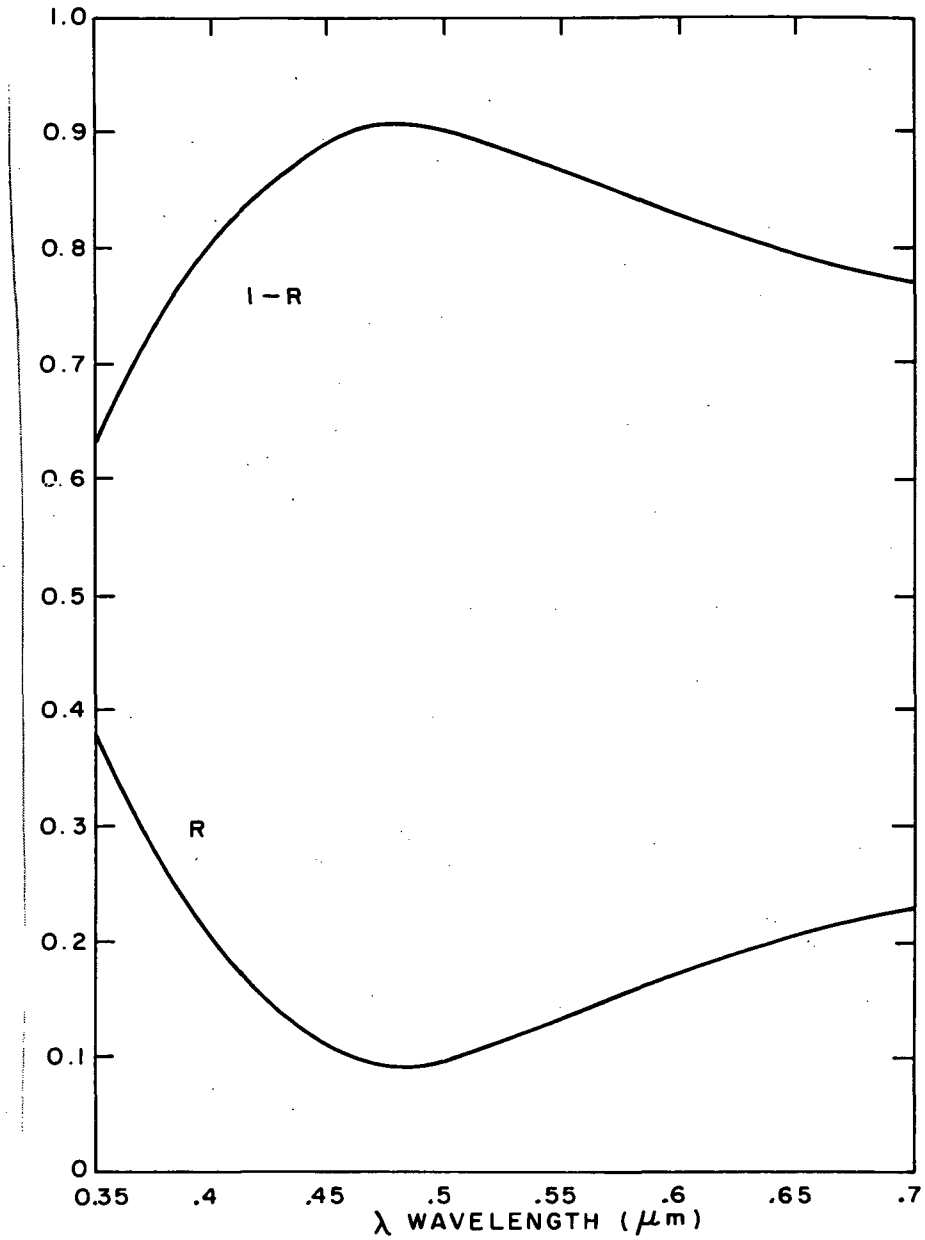

Figure 27. Measured reflection coefficient for 700-Å Al_2O_3 AR coating as a function of wavelength.

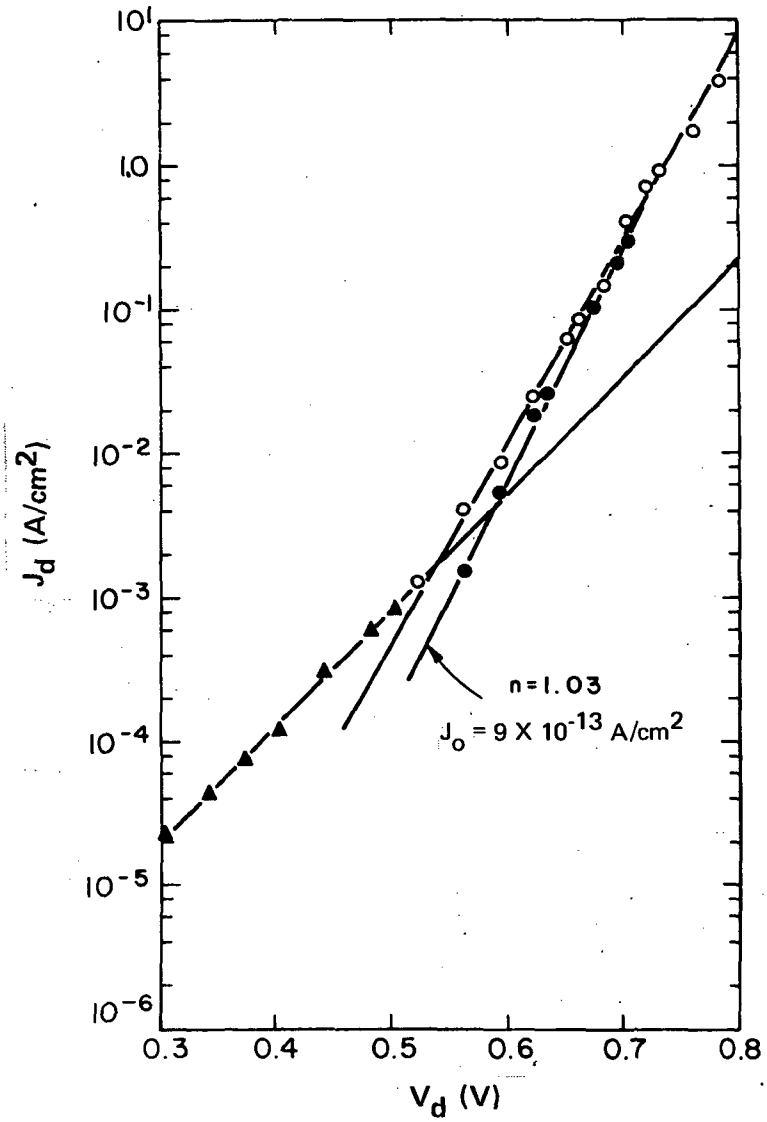

Figure 28. Dark I-V characteristic for epitaxial diode #729090.

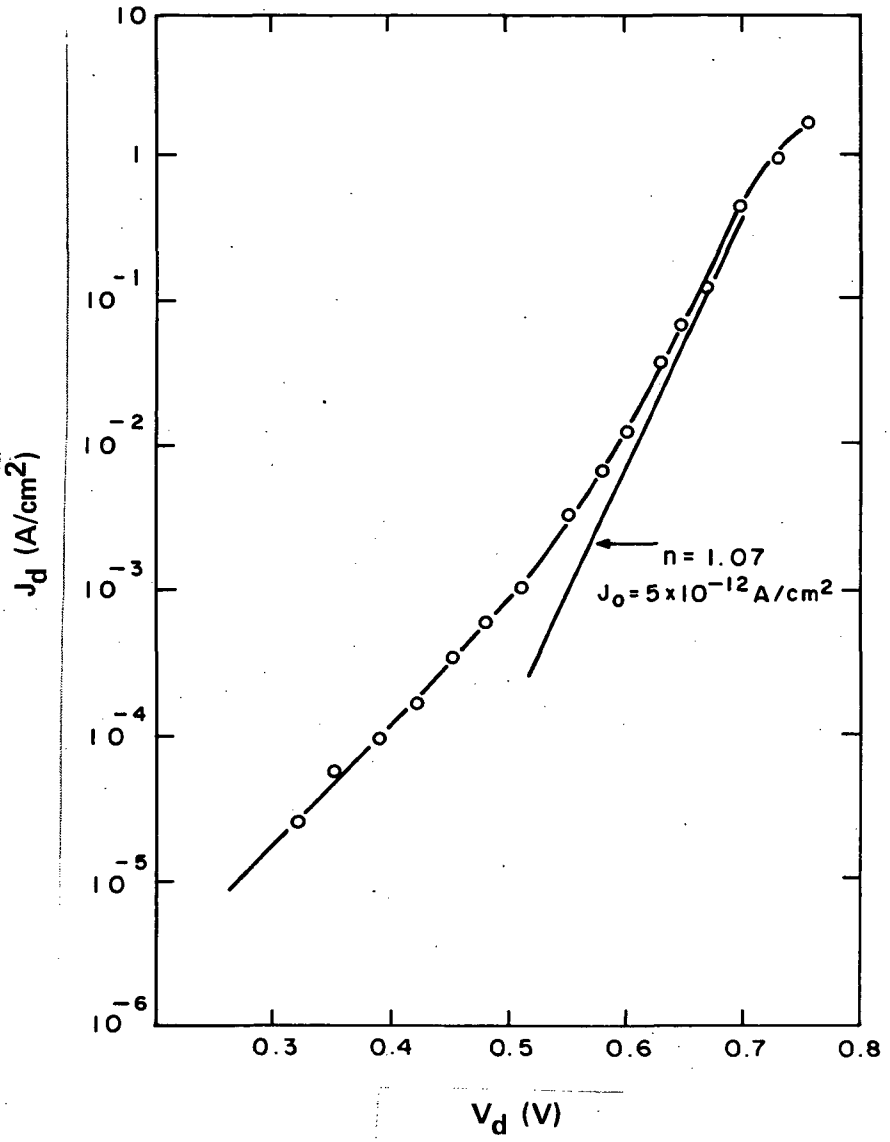

Figure 29. Dark I-V characteristics for epitaxial diode #665996-2.

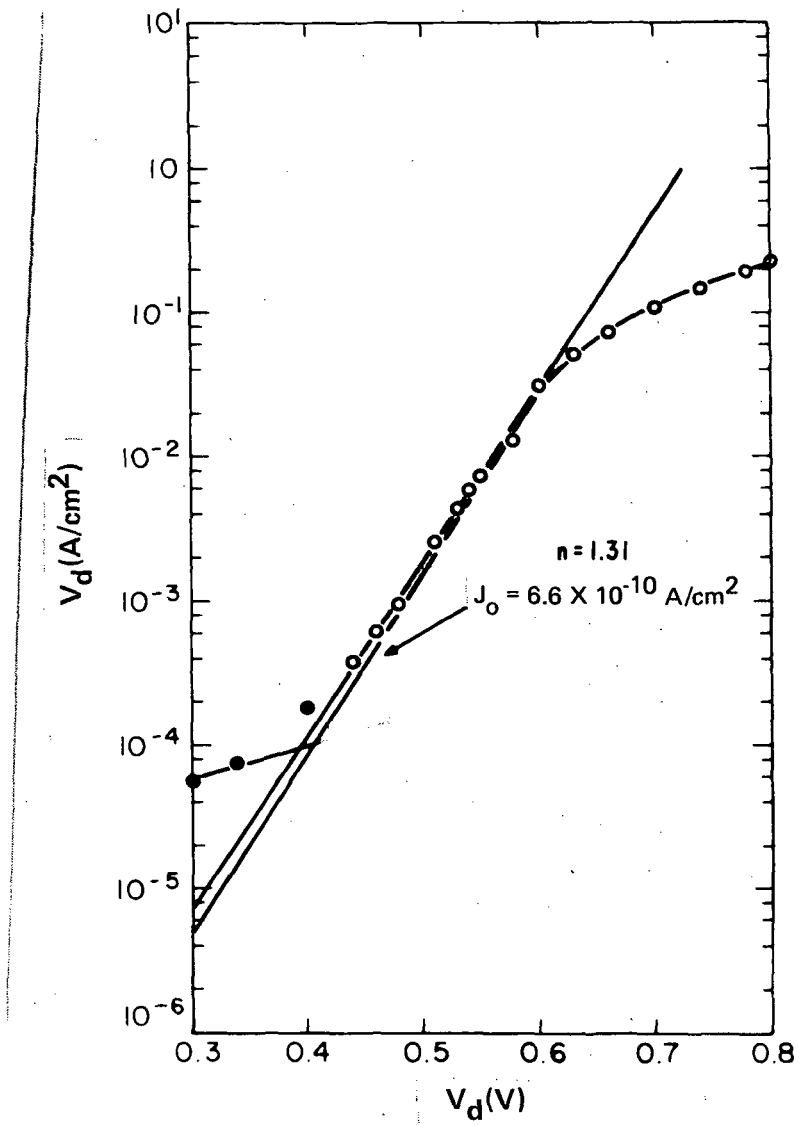

Figure 30. Dark I-V characteristic for p^+/n diffused diode.

it represents a slight loss in efficiency. The origin of these currents and methods of reducing them were not studied under this contract and thus represent an area for further investigation.

The moderate short-circuit current densities ($\sim$25 mA/cm^2 under AM-1 illumination) obtained with all epitaxial cells indicate an area for efficiency improvement. In addition to excessive metallization and surface reflection, our best cells were only $\sim$40 μm in total thickness. Thicker cells with graded profiles should result in increased collection of carriers generated at longer wavelengths yielding higher short-circuit current.

As a final, but very important point, in the epitaxial cells reported here, surface layer thicknesses ranged from a low value of 1 μm to 4 μm. These values are quite large when compared with the 0.1- to 0.2-μm junction depths commonly used in high-efficiency diffused cells. Although very high short-circuit currents were not obtained, moderately high efficiencies (12.5%) and very high open-circuit voltage (636 mV) were achieved, and it is anticipated that improvements in short-circuit current are possible by proper surface treatment and surface layer profiling. With these improvements, the epitaxial method would alleviate the major difficulties of reproducibility and high sheet resistance associated with extremely shallow diffused junctions.

VI. CELLS FABRICATED WITH A SINGLE EPITAXIAL LAYER ON BULK SILICON

A. Objectives and Method

The objective of this work and the method of cell fabrication differ from the experiments reported in the previous sections. The major objective is to study junctions and solar cells formed by the growth of a single epitaxial layer on bulk silicon wafers and to observe the solar cell parameters, in particular open-circuit voltage, as a function of the bulk silicon resistivity and epitaxial surface layer thickness. Both n- and p-type <111> oriented, float-zone (FZ) silicon wafers with nominal resistivities of 0.1, 1, and 10 Ω-cm were used* as the substrates for the epitaxial layers. Junction depths of 0.3, 1, and 3 μm with a surface concentration of $\sim 5 \times 10^{19}$ A/cm^{-3} were studied. These layers were grown by the pyrolytic decomposition of silane as described in Section II-B of this report. Solar cells and mesa diodes were fabricated and evaluated by similar methods described for the p/n/n$^+$ structures.

As a baseline for these studies, diffused n$^+$/p and p$^+$/n cells were also fabricated by direct diffusion of phosphorus and boron into the same type bulk wafers.

B. Experimental Results - Summary

A matrix of 18 epitaxial samples was completed, comprising grown junctions of 0.3, 1, and 3 μm on bulk n- and p-type silicon of ~0.1, 1, and 10 Ω-cm. In addition, three diffused cells were fabricated for comparison. Small area mesa diodes (1.7×10^{-2} cm^2) and solar cells (2.18 cm^2) were fabricated and evaluated. The cell grid pattern and geometry are the same as that shown in Figs. 14 and 15. Metallization is Cr/Au for top grid pattern and Cr/Ni for back contact. An AR coating of 750 Å Al_2O_3 was evaporated on all cells.

The quality of the epitaxial junctions and cell efficiency varied widely, with the n$^+$/p cells showing consistently better performance. The highest efficiency was 8.3% (AM-1) for an n$^+$/p cell with a 1-μm junction depth on a 10-Ω-cm p-bulk wafer.

In general, the junction quality deteriorated for the 0.1-Ω-cm samples, resulting in lower fill-factors and open-circuit voltages than would theoretically be expected for this bulk resistivity.

*Obtained from the Wacker Chemical Co.

The diffused cells showed slightly better performance, with a maximum AM-1 efficiency of 10.2% for an n^+/p (0.1 Ω-cm) sample.

C. Electrical Characteristics

For each sample, solar I-V characteristics were measured; dark I-V curves and lifetimes were obtained on the cells and diagnostic diodes. A summary of the solar cell performance for the epitaxial and diffused cells is given in Table V. Several conclusions can be drawn from these data: (1) Epitaxial junctions grown directly on bulk silicon by the pyrolytic decomposition of silane are not better than those obtained by diffusion into the same material. (2) The difficulties of obtaining high open-circuit voltage and good diode characteristics on highly doped bulk samples ($\rho_{bulk} \gtrsim 0.1$ Ω-cm) are *not* alleviated by this epitaxial method. (3) The n-type (P + As) epitaxial layers on p-bulk form a better-quality junction than the p^+ (boron) junctions.

Focusing, for example, on the 0.16-Ω-cm p-bulk samples of 0.3-μm junction depth, we see that the diffused cell has higher efficiency (10.2% vs 5.9%), higher fill-factor (0.70 vs 0.61), and higher short-circuit current density (24 mA/cm^2 vs 16.6 mA/cm^2) than the epitaxial cell. The dark I-V characteristics for these cells and one adjacent diode are shown in Figs. 31 and 32, where it is seen that the n factor and saturation current density are closer to ideal for the diffused junction. It should also be noted that there is a higher leakage current density in the cells than in the small diodes, and that this is more pronounced in the epitaxial case.

For comparison of the effect of background doping level and junction depth, the dark I-V characteristics for epitaxial n^+/p samples of 10-Ω-cm resistivity with junction depths of 0.3 μm and 3 μm are shown in Figs. 33 and 34. At the same junction depth (0.3 μm) as for Fig. 31, it is seen that the I-V characteristics for the cell and diode are improved over the 0.16-Ω-cm background doping level. A more significant improvement is seen in Fig. 34 for the 3-μm junction depth into 10-Ω-cm material. This cell had the highest fill-factor (0.81).

The p^+/n junctions were of poorer quality than the n^+/p junctions; see Fig. 35.

D. Open-Circuit Voltage

The simple theory of an ideal n^+/p (bulk) junction shows that the open-circuit voltage (V_{oc}) increases at the rate of 60 mV for each decade increase in bulk carrier concentration. That this rate of increase

TABLE V. SUMMARY OF SOLAR CELL PERFORMANCE FOR SINGLE EPITAXIAL LAYERS AND DIFFUSED CELLS

n+ Epi/p Bulk							p+ Epi/n Bulk						
x_j (μm)	ρ_p (Ω-cm)	N_A (A/cm^3)	V_{oc} (mV)	J_{sc} (mA/cm^2)	η (%)	F.F.	x_j (μm)	ρ_n (Ω-cm)	N_D (A/cm^3)	V_{oc} (mV)	J_{sc} (mA/cm^2)	η (%)	F.F.
0.3	0.16	2E17	560	16.6	5.9	0.61	0.3	0.38	1.4E16	490	22.3	7.0	0.63
0.3	1.7	8E15	528	20.0	8.0	0.73	0.3	1.4	3.7E15	446	19.0	5.7	0.65
0.3	10	2E15	500	20.0	7.0	0.68	0.3	12.1	4E14	470	23.0	7.1	0.64
1	0.16	2E17	571	18.8	7.0	0.64	1	0.38	1.4E16	400	21.3	-*	-
1	1.7	8E15	533	21.0	6.6	0.58	1	1.4	3.7E15	326	12.0	-	-
1	10	2E15	506	22.0	8.3	0.72	1	12.1	4E14	370	10.0	-	-
3	0.16	2E17	592	14.7	6.4	0.71	3	0.38	1.4E16	532	17.2	6.1	0.65
3	1.7	8E15	540	15.7	6.8	0.75	3	1.4	3.7E15	508	14.4	500	0.66
3	10	2E15	506	16.4	7.0	0.81	3	12.1	4E14	500	12.0	4.1	0.67
n+ Diff./p bulk							p+ Diff./n bulk						
0.25	0.16	2E17	582	24.4	10.2	0.70	0.3	1.5	3.5E15	530	28.0	10.4	0.67
0.3	1.7	8E15	546	20.7	8.0	0.68							

*Excessive leakage.

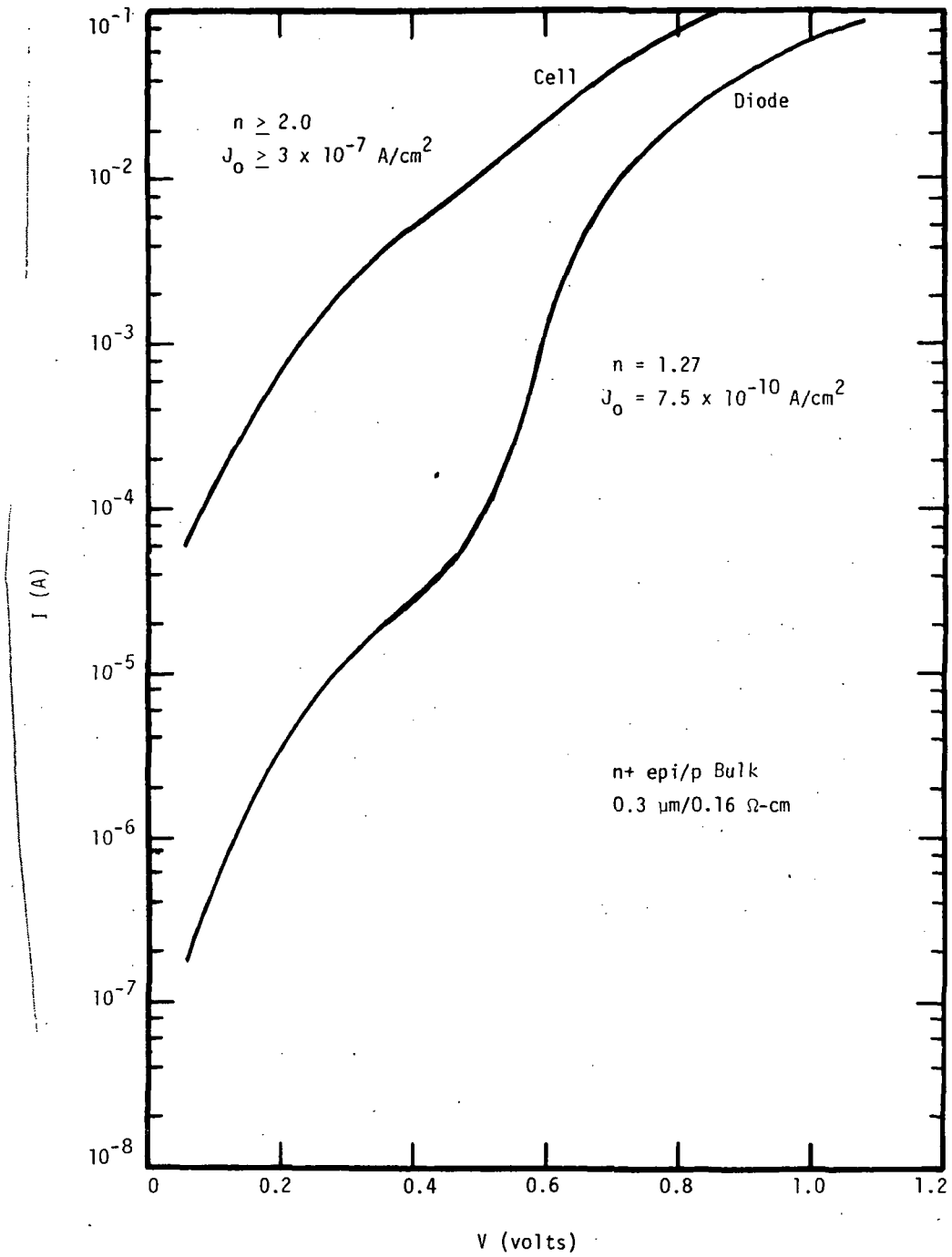

Figure 31. I-V characteristics for n^+(epi)/p(bulk) solar cell and mesa diode. p-bulk resistivity = 0.16 Ω-cm.

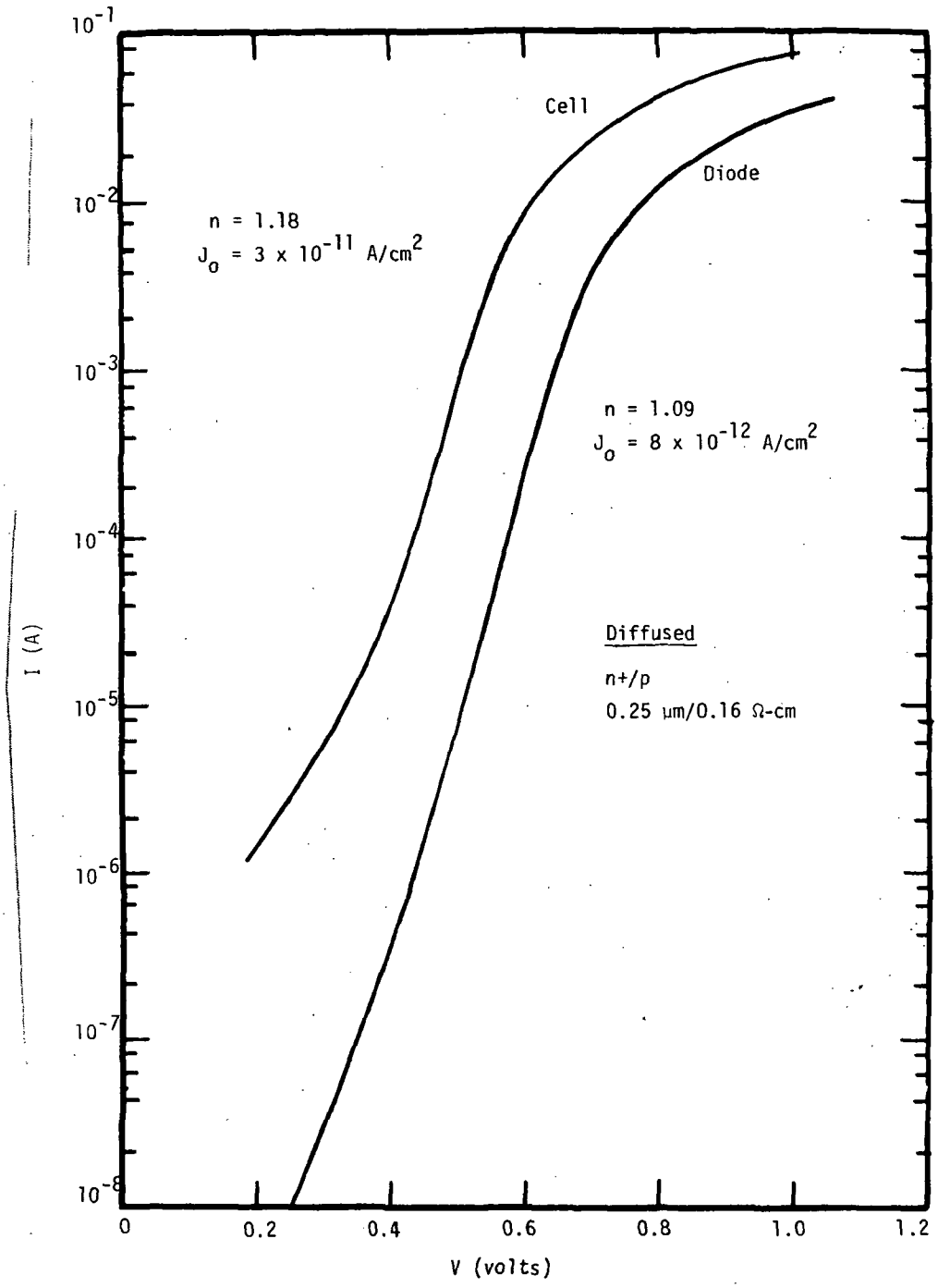

Figure 32. I-V characteristics for diffused n^+/p(bulk) solar cell and mesa diode. p-bulk resistivity = 0.16 Ω-cm.

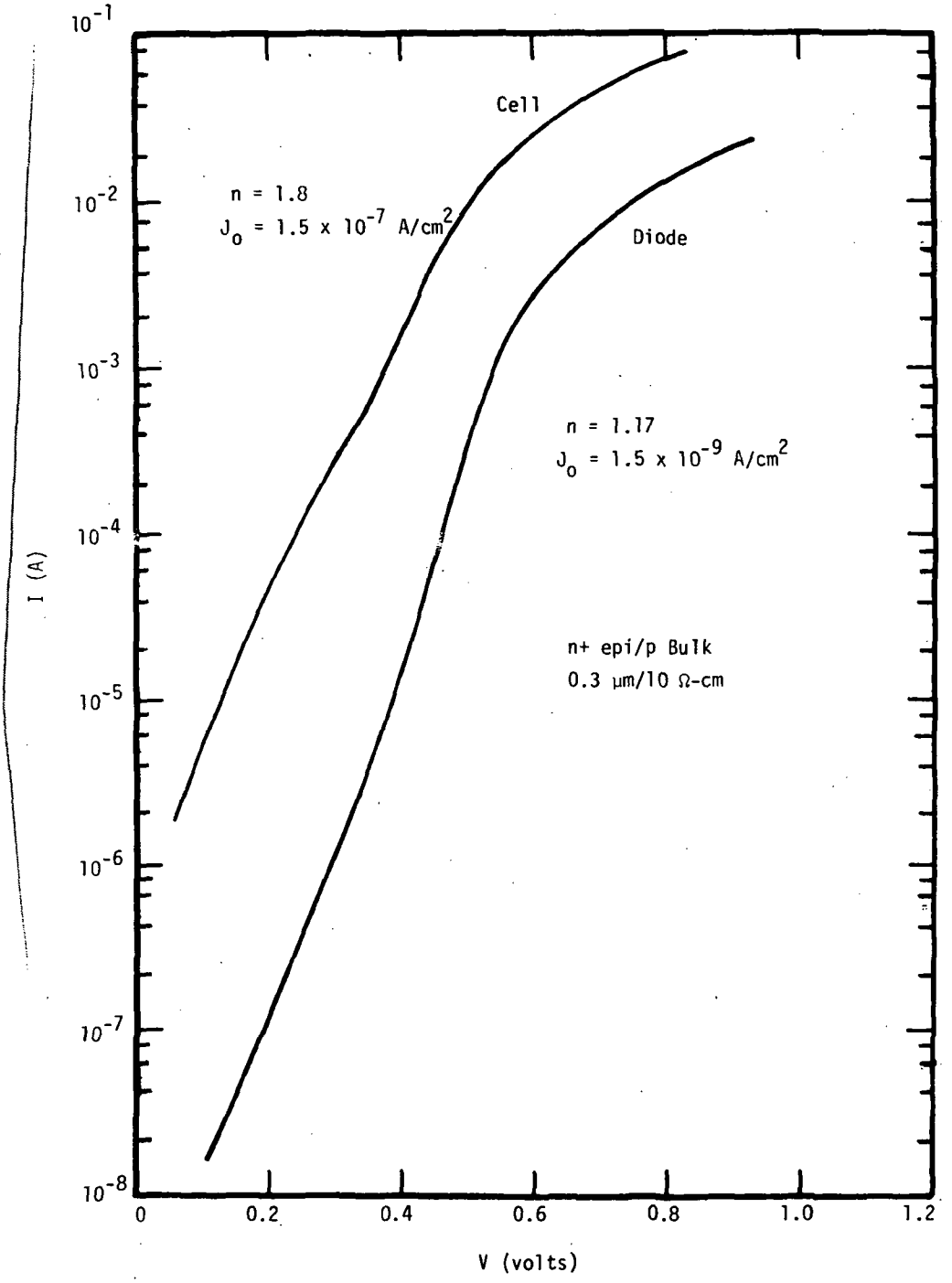

Figure 33. I-V characteristics for n^+(epi)/p(bulk) solar cell and mesa diode. p-bulk resistivity = 10 Ω-cm. n^+ thickness = 0.3 μm.

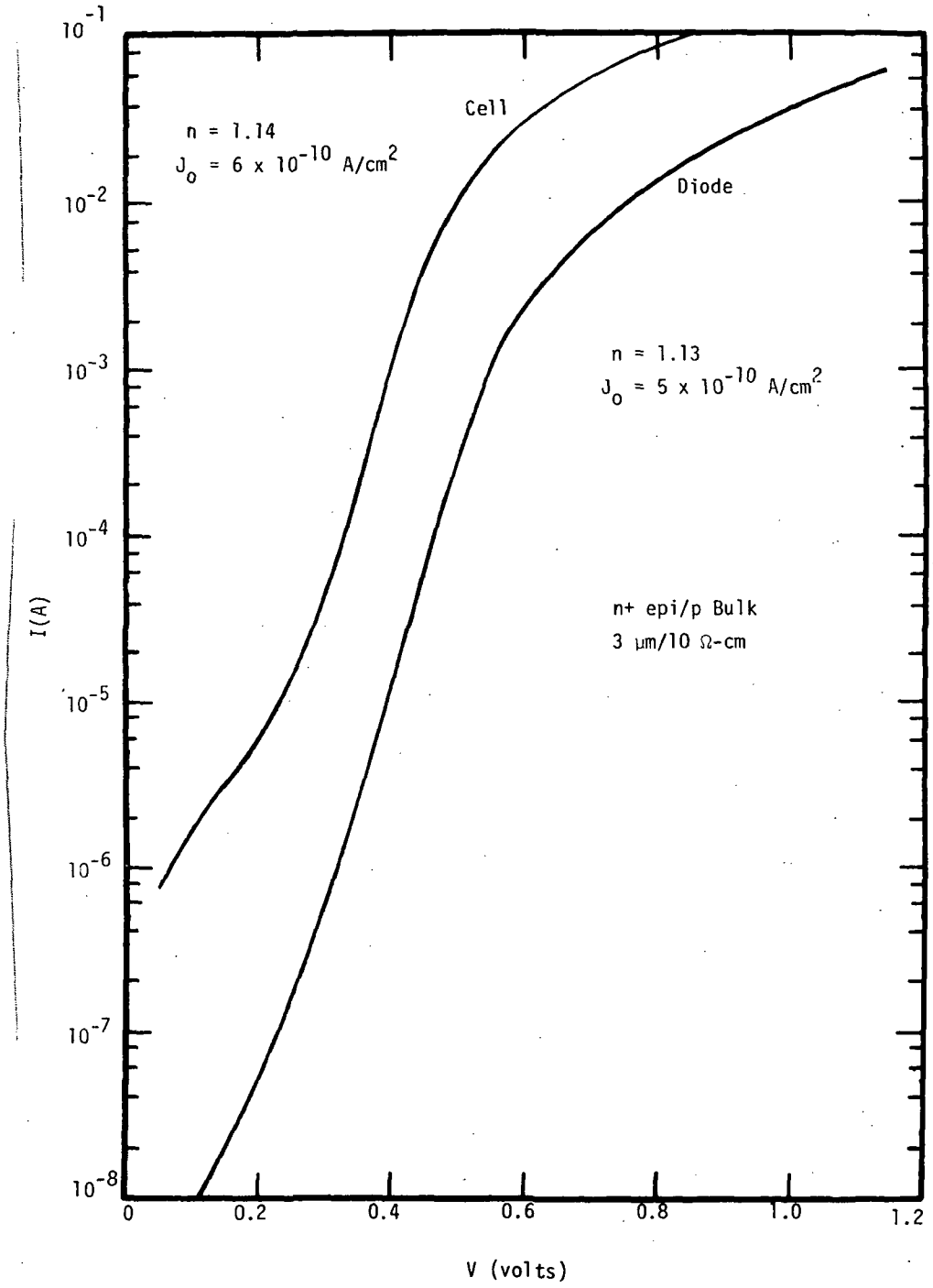

Figure 34. I-V characteristics for n^+(epi)p(bulk) solar cell and mesa diode. p-bulk resistivity = 10 Ω-cm. n^+ thickness = 0.3 μm.

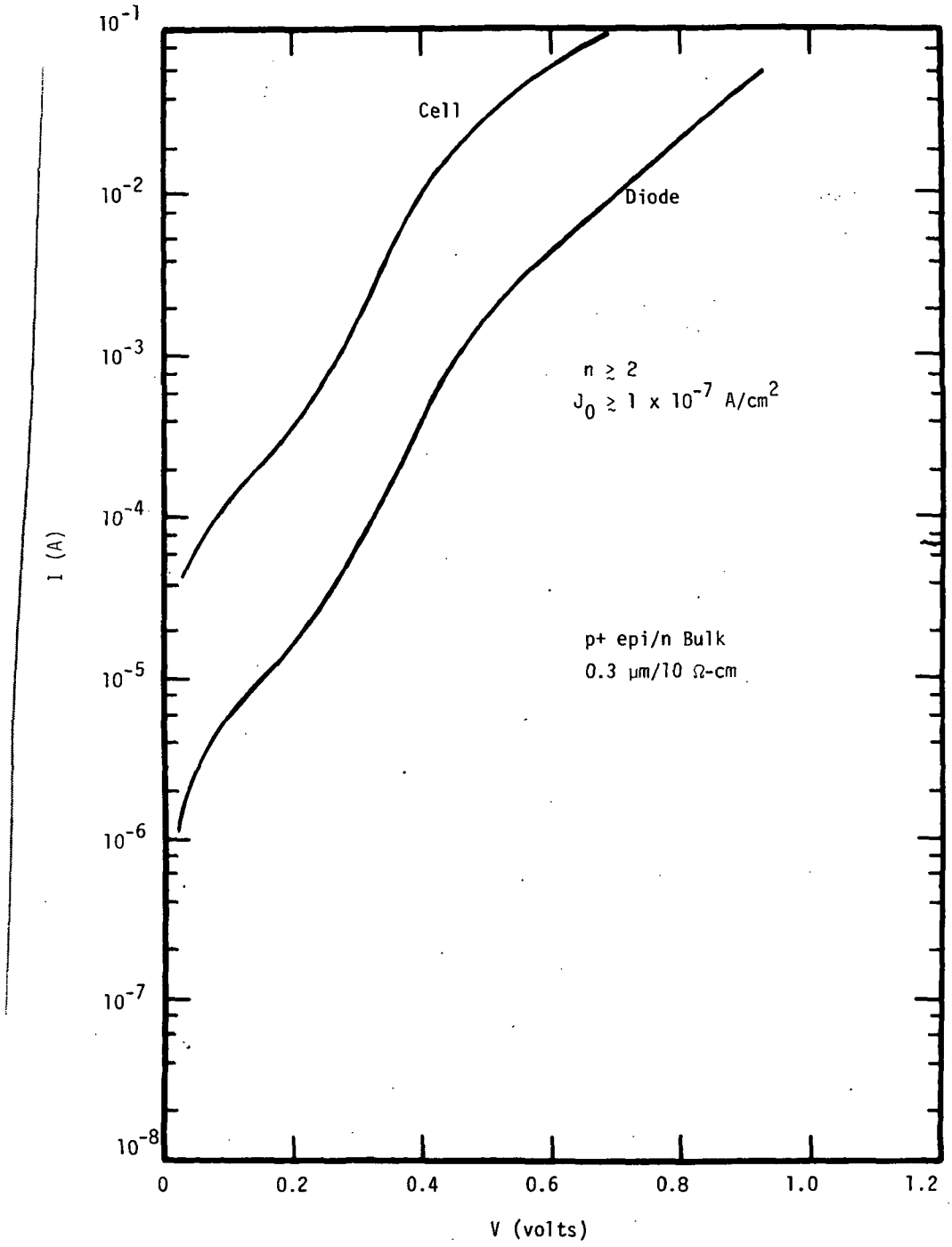

Figure 35. I-V characteristics for p^+(epi)/n(bulk) solar cell and mesa diode. n-bulk resistivity = 10 Ω-cm. p^+ thickness = 0.3 μm.

does *not* occur for the epitaxial n^+/p cells is shown in Fig. 36, where the average V_{oc} for the nine n^+/p solar cells is plotted versus the bulk background acceptor concentration. It is seen that the increase in open-circuit voltage begins to fall below the theoretical 60 mV/decade as the base resistivity decreases toward 0.16 Ω-cm.

That defects in the vicinity of the junction begin to affect cell performance for low bulk resistivities is evidenced by an examination of the dark I-V characteristics which reveals that the 0.16-Ω-cm samples have dominant recombination and shunting currents (slope $n \tilde{=} 2$) up to 535 mV, a value 100 to 150 mV higher than that of the 10-Ω-cm samples.

These results are similar to the experiences of other workers (refs. 8,22) who have studied diffused cells in low-resistivity bulk silicon, and indicate that the mechanisms which limit open-circuit voltage and cell performance are *not* alleviated by the particular epitaxial technique used here.

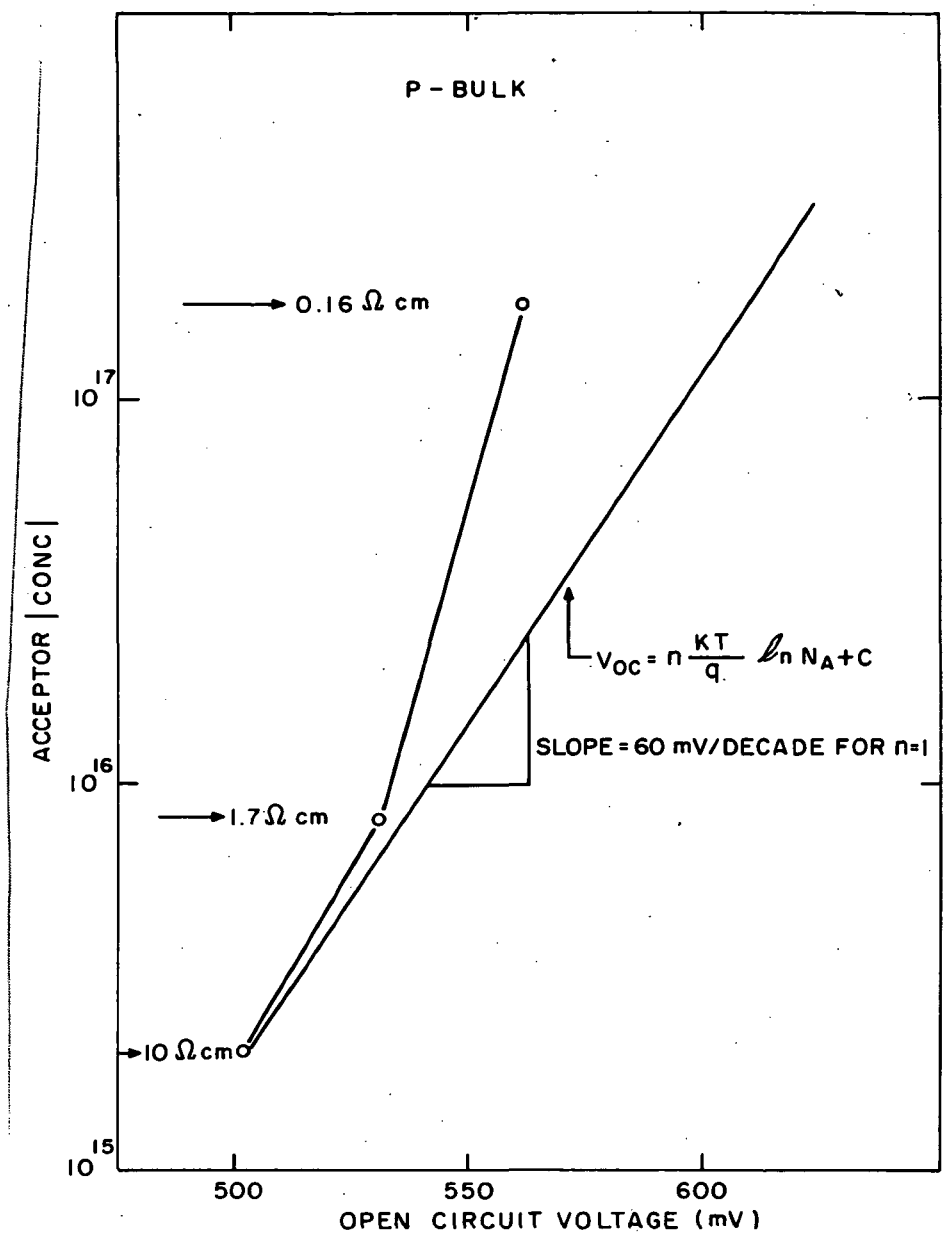

Figure 36. Comparison of measured and theoretical open-circuit voltage as a function of bulk, base layer carrier concentration for n^+(epi)/p solar cells. Each data point is an average of three cells.

VII. CONCLUSIONS

A. Epitaxial Solar Cells Fabricated Using Dichlorosilane

The major conclusions drawn from the work conducted under this contract may be summarized by the following list of attributes which we have observed concerning epitaxial junctions, layers, and solar cells:

(1) The epitaxial method offers a degree of flexibility in profile tailoring which allows for the optimization of solar cell structures. This has been demonstrated in our work by the use of intentionally graded base layers, which yielded solar cells with record-high open-circuit voltage.

(2) Good quality junctions are formed by the epitaxial method with nearly ideal current-voltage characteristics. This results in high open-circuit voltage and high fill-factor. We have fabricated epitaxial junctions with the n factor equal to 1.03 and saturation current density as low as 9×10^{-13} A/cm^2.

(3) Moderately high efficiency cells can be made without resorting to very shallow junctions. We have fabricated epitaxial cells having 4-μm surface layers, which yielded an AM-1 efficiency of 10.9%. Cells with 1-μm surface layers were 12.5% efficient, which should be compared with commercial diffused cells that typically have 0.15- to 0.5-μm diffused layer thickness. Thicker surface layers with lower sheet resistance would allow a greater flexibility in future cell designs.

(4) In addition, although not specifically studied under this contract, it is anticipated by the work reported on thin cells (ref. 6) that epitaxial cells will show good resistance to the damage caused by radiation in space applications.

We have found that the method of growth of silicon layers using dichlorosilane is a reliable and reproducible method for the formation of solar cell structures. High growth rates were achieved without sacrificing material quality. Most cell structures were grown at 5 μm/min so that a typical cell of ∿50-μm thickness can be grown in 10 minutes. Growth rates as high as 16 μm/min were demonstrated without degradation in lifetime. Control and reproducibility of resistivity profiles were obtained by metering the dichlorosilane in gaseous form. This method is adaptable to automated, computer-controlled processing techniques.

B. Cells Fabricated by the Growth of Single Epitaxial Layers on Bulk Silicon - Silane Process

Our studies of single epitaxial layers forming a junction on bulk silicon wafers have shown that the open-circuit voltage does not increase as rapidly with decreasing bulk resistivity as the theory predicts. We have found that the junction I-V characteristics degrade as the bulk resistivity approaches 0.1 Ω-cm, indicating that defects are present in the vicinity of the junction. This resulted in poor solar cell characteristics of the highly doped material, in agreement with previously reported work using diffusion technology.

VIII. RECOMMENDATIONS

In order to realize the full potential of the epitaxial method of solar cell fabrication, a number of areas should be explored in greater detail. Since high open-circuit voltage and good fill-factors were achieved with only moderate short-circuit current density (J_{sc}), methods for increasing J_{sc} should be explored. Modest increases ($\sim$10%) over the present cell response can be obtained with improved antireflection coatings and minimized metal coverage. To obtain substantial improvement, J_{sc} at AM-1 $\sim$33 mA/cm^2, surface-layer profiles should be explored in greater detail. Intentional surface-layer gradients put in by epitaxy and diffusion should be experimentally studied.

A study of thicker base-layers containing gradients is recommended for improved infrared response. In addition, further studies of a range of gradients in both surface and base-layers should be made for optimization of cell response.

A. Evaluation of Gradients in Base and Surface Layer of Epitaxial Silicon Solar Cell Structures

1. Base layer gradients. An expanded study of the effect of gradients in the doping profile of base layers on solar cell performance. Examination of thickness as well as doping levels should be made with thickness ranging from approximately 10 μm to 100 μm, and doping levels at the junction ranging from 10^{15} to 10^{17} A/cm^3.

2. Surface layer profiles and gradients. To study the effects of gradients grown epitaxially into the surface layer of both n/p and p/n solar cell structures. More emphasis should be placed on n/p cells. Both thin ($\sim$0.2 μm) and thick ($\sim$5 μm) surface layers should be examined.

B. Fabrication and Evaluation of Solar Cells

1. Solar cell fabrication. Using the information gained from Section A, above, thin ($\leq$10 μm) and thick ($\sim$100 μm) solar cell structures should be studied. Gradients in the base layers and/or surface layers should be grown to optimize open-circuit voltage, short-circuit current, and efficiency.

2. Radiation damage. The effect of radiation on epitaxial cells should be studied to determine their suitability for space applications. Experiments should be made with both n/p and p/n cells.

3. Cell and material evaluation. The solar cell structures should be examined by the techniques described below to characterize the junction and the surface layer profile so as to relate the structural and electrical properties to the solar cell performance.

(1) Capacitance spectroscopy. To determine the presence and type of deep level traps which limit lifetime and affect I-V characteristics.
(2) Scanning electron microscopy - (EBIC). To determine the uniformity of epitaxial layers, set limits on large area cells, and identify defects which degrade cell performance.
(3) Plasma resonance, surface C-V, and spreading resistance. These methods should be employed as needed in an attempt to characterize the impurity profile in the thin top layers.

APPENDICES

APPENDIX A

SOLAR SIMULATOR MEASUREMENTS

Indoor testing of the cells was conducted with the apparatus shown in Fig. 37. The GE ELH lamp was calibrated for spectral output at regulated lamp voltages of 90, 100, and 110 V using an EG&G PV 444A photodetector and narrow-band optical filters at a distance of 30.5 cm. Response curves taken at each voltage compared with an approximate AM-1 spectrum are shown in Fig. 38.

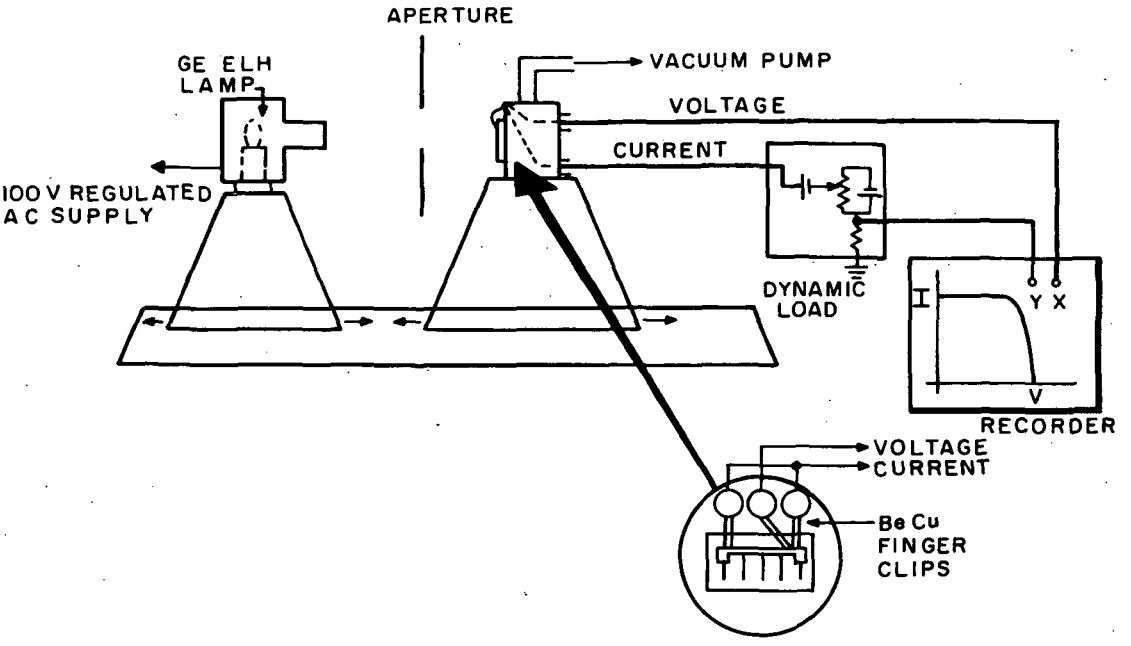

Figure 37. Solar AM-1 simulator and cell mount.

The output was also measured as a function of distance from the lamp over the range 10 to 60 cm and was found to vary as one over the distance squared, as expected. This would allow for measurement of cells at different intensities with the same spectral content.

For solar cell measurements, it was decided to operate the lamp at 100 V to prolong the lamp life (expected life at 110 V is 30 h). The integrated spectral power at a distance of 30.5 cm, when operating at 100 V, is 99 mW/cm^2. However, the lamp output, when compared with the AM-1 spectrum, is higher in the orange-red and lower in the blue-violet.

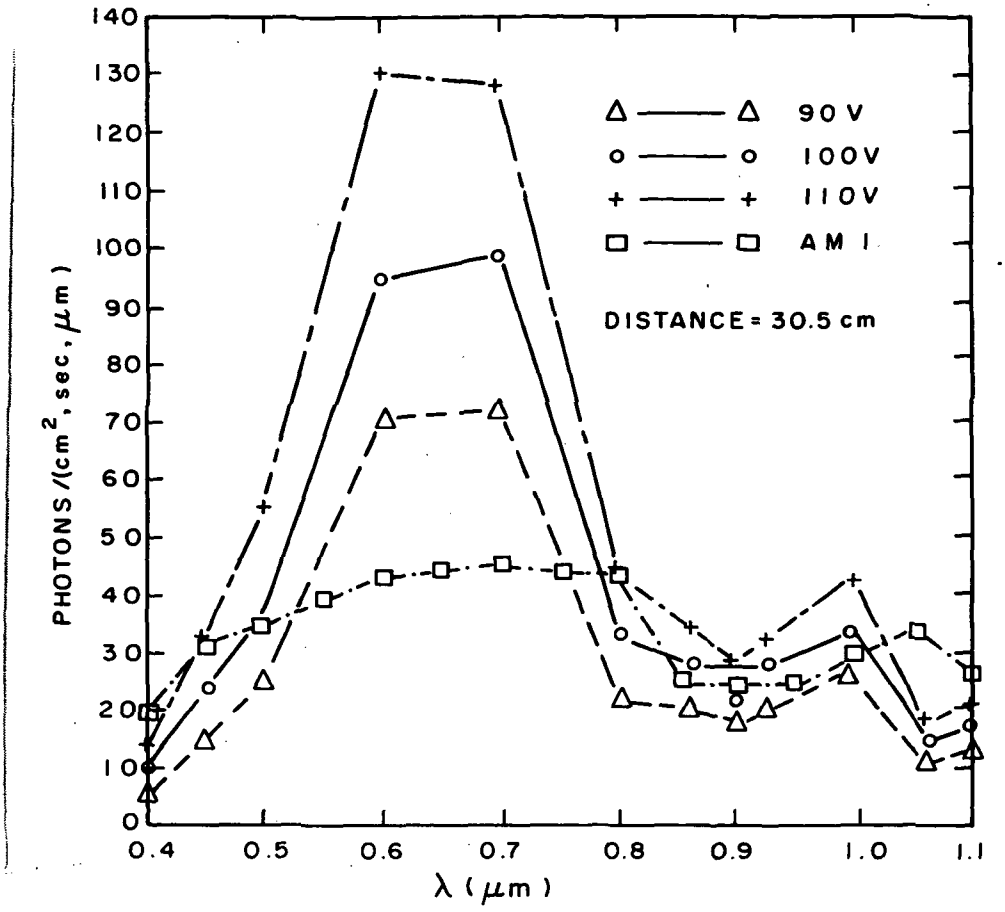

Figure 38. Output response curves for GE ELH lamp compared with simplified AM-1 spectrum.

The cell holder shown in the inset of Fig. 37 is a goldplated copper block with holes for vacuum holddown of solar cells. For temperature stability a thermoelectric cooler and cooling fins (not shown) are mounted on the rear of the block. The fingerclip arrangement is a balanced current, modified (common-ground) four-point contact. The balanced current contacts to each end of the cell cancels bus-bar voltages and tends to keep the current distribution uniform over the cell area.

The dynamic load shown is used to measure cell current and provide offset voltages for open-circuit and short-circuit current measurements.

For calibration purposes a secondary standard cell provided by the NASA-Lewis Research Center was measured prior to each run. Measurements were made at 27°C.

Spectral response measurements were made by inserting a filter wheel containing narrow-band calibrated optical filters between the lamp and detector. To determine quantum efficiency (electron/incident photon), the light is chopped at 520 Hz, and the voltage developed across a 100-Ω load in parallel with the detectors is measured as a function of wavelength using a lock-in amplifier. The detector used was an EG&G PV 444-A photocell, supplied with certified quantum efficiency. The quantum efficiency of solar cells was obtained by taking the ratio of the voltage developed across the test cell at each wavelength to the voltage of the EG&G PV 444-A detector.

APPENDIX B

LIFETIME MEASUREMENTS

All of the lifetime data presented in the body of this report were obtained by two junction recovery techniques: (1) open-circuit voltage decay (ref. 23) and (2) reverse recovery method (ref. 24). These methods are briefly discussed here with a description of the equipment used in the measurements.

Both of these methods are useful in the case of solar cells as they measure a lifetime of minority carriers injected by the junction after fabrication, so that the lifetime measured relates to the final structure.

1. Open-Circuit Voltage Decay. - A schematic representation of the basic circuit for open-circuit voltage decay measurement with a sketch of the output voltage is shown in Fig. 39. For $t < 0$ the switch is

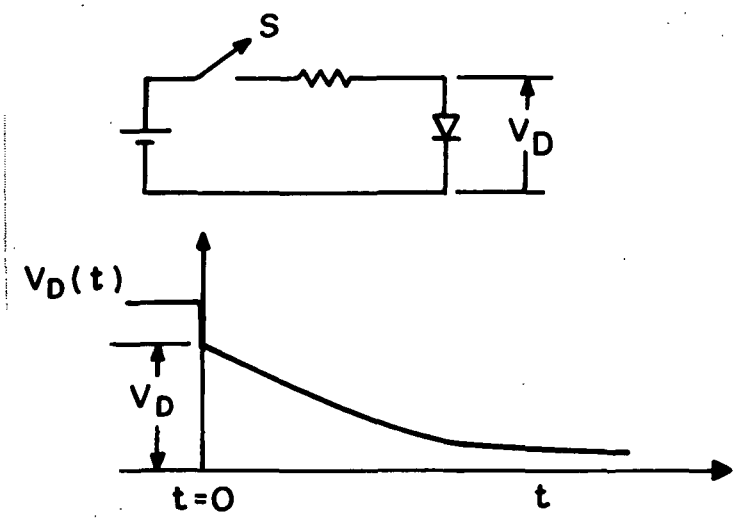

Figure 39. Schematic circuit and waveform associated with open-circuit voltage decay method of lifetime measurement.

closed and the junction under test is forward-biased to a voltage V_o. For a p^+/n junction, the minority hole concentration in the n region is assumed to reach a steady-state value of p_n before $t = 0$. At $t = 0$,

the switch is opened and the junction remains forward-biased; the hole density is now a function of time

$$p = p_n + \Delta p(t) \tag{B1}$$

where from the usual junction theory

$$p = p_n \exp[qV/nkT] \tag{B2}$$

and V is the instantaneous junction voltage.

If the assumption* is made that the excess carrier concentration, Δp, decays exponentially with time according to a single effective lifetime τ_p, then

$$\Delta p = \Delta p_o e^{-t/\tau_p} \tag{B3}$$

Combining Eqs. (B1), (B2), and (B3), and solving for the junction voltage

$$V(t) = \frac{nkT}{q} \ell n \left[1 + \frac{\Delta p_o}{p_n} \exp(-t/\tau_p)\right] \tag{B4}$$

where Δp_o is related to the junction voltage at t = o by

$$V_D = \frac{nkT}{q} \ell n\ 1 + \frac{\Delta p_o}{p_n} \tag{B5}$$

For $t/\tau_p << 1$ and if V_D is >> than the thermal voltage, kT/q, Eq. (B-4) may be approximated by

$$V(t) = V_D - \frac{nkT}{q} t/\tau_p \tag{B6}$$

The initial voltage variation is linear in time with the slope inversely proportional to the lifetime, τ_p. τ_p is then given by

$$\tau_p = \frac{nkT}{q} \left(\frac{dV}{dt}\right)^{-1} \tag{B7}$$

*This assumption and the subsequent approximations may be more rigorously justified. See, for example, B. Lax and S. F. Neustader, J. Appl. Phys. 25, 1148 (1954).

Equation (B7) is the basic relationship used to obtain the lifetime from an oscilloscope trace of the diode voltage vs time.

The above simplified theory does not take high injection effects into account and assumes moderate injection conditions. Also, generation in the space charge region and diffusion effects are neglected.

We have found that most junctions measured have a linear voltage decay, and provided that the n factor is first determined from forward I-V measurements, the lifetime obtained by this method agrees well with that obtained by the reverse recovery method described below.

2. Reverse Recovery Method. - The basic circuit and waveforms for this method of lifetime measurement are shown in Fig. 40. The junction is forward-biased to a current, I_F, by supply V_1, then at t = 0, the junction is reverse-biased by supply V_2. The amount of forward and reverse biases is adjustable with R_1 and R_2. Under the assumption of a single lifetime, τ_p, the storage time T_s is a function of τ_p, I_F/I_R and the amount of stored charge remaining at the end of the storage phase T_s.

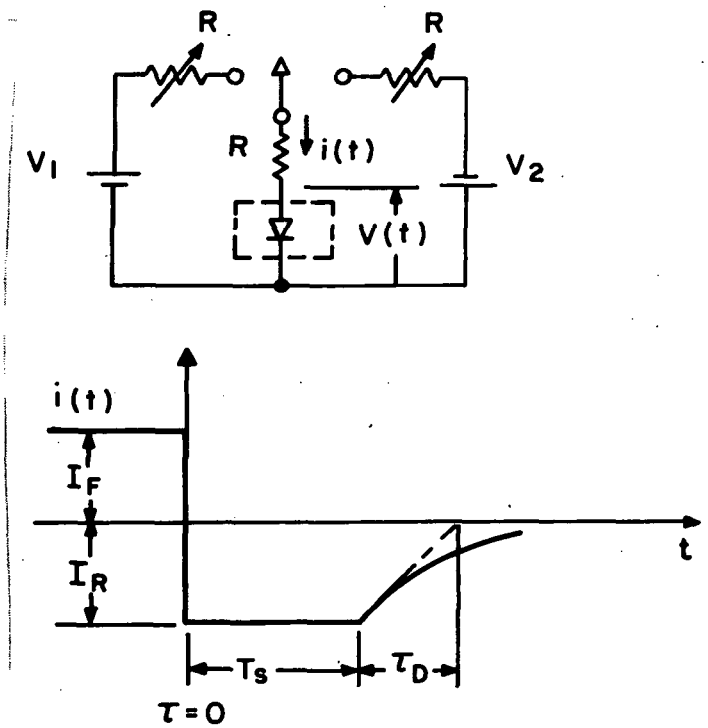

Figure 40. Circuit and waveform associated with the reverse recovery method of lifetime measurement.

The method we have used for extracting lifetimes from measurements of T_s as a function of I_F/I_R is described by Kuno (ref. 24). The relationship between T_s and τ_p, is given by Kuno,

$$T_s = \tau_p \left[\ell n(1 + I_F/I_R) - \ell n(1 + \tau_R/\tau_p) \right] \qquad (B8)$$

where τ_R is related to the amount of charge remaining in the base region of the junction at $t = T_s$.

If T_s is plotted as a function of $\ell n(1 + I_F/I_R)$, a straight line with slope τ_p will result. Examples of data taken on solar cell structures having 1.3-μs and 13.2-μs lifetimes are shown in Figs. 41 and 42.

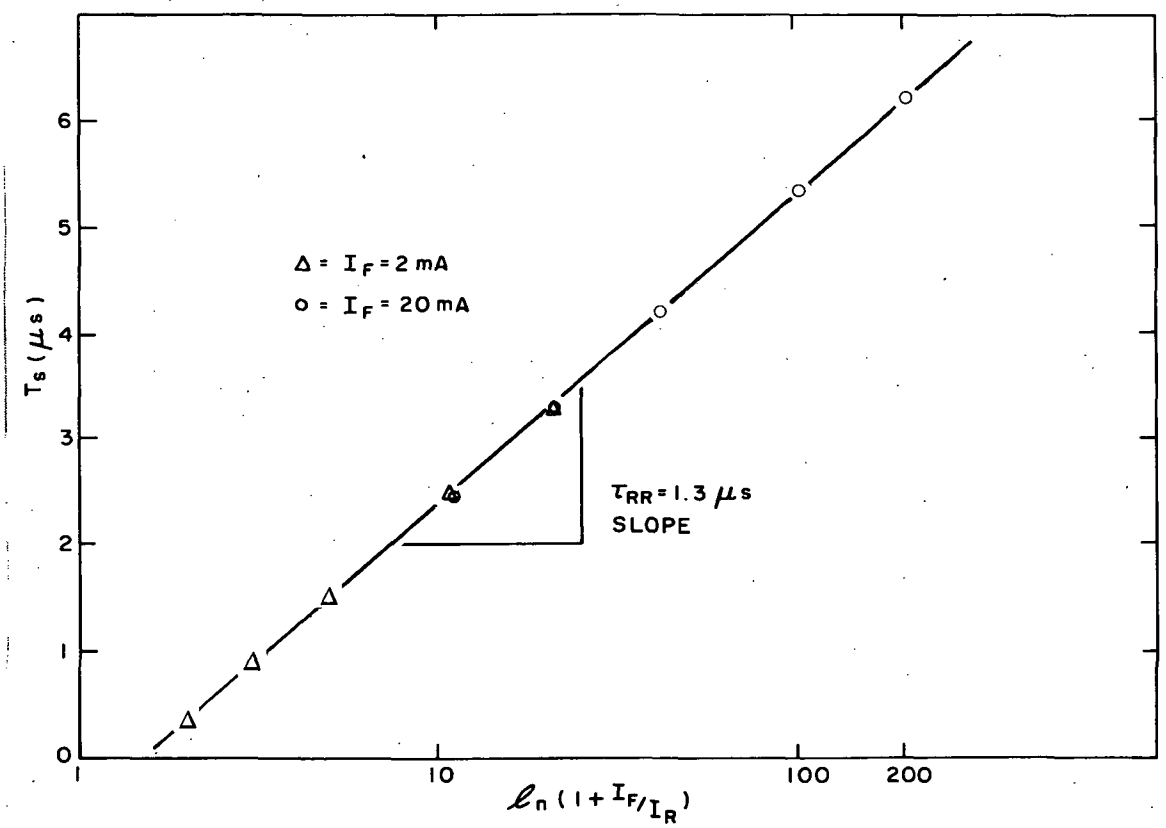

Figure 41. Data representing measurement of lifetime by reverse recovery method for a lifetime of 1.3 μs.

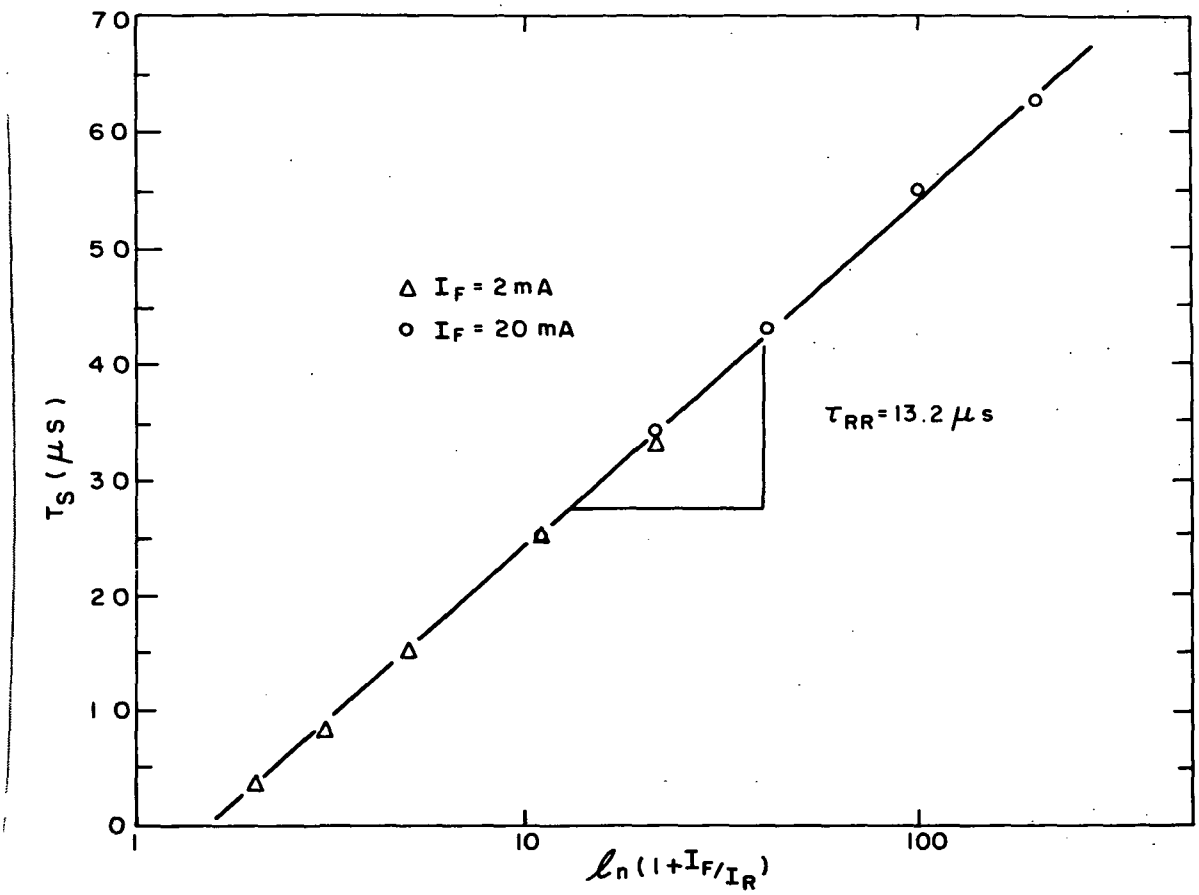

Figure 42. Data representing measurement of lifetime by reverse recovery method for a lifetime of 13.2 μs.

We have found good agreement (∿10%) between the two methods described here. In addition, we have found that the relative order of the measured lifetimes for solar cells is in agreement with the infrared spectral response, i.e., cells with longer lifetime have higher quantum efficiency at long wavelengths.

3. Apparatus for Lifetime Measurement. - We have found that the Tektronix type S "Diode Recovery" plug-in is very suitable for rapid measurement of both open-circuit decay and reverse recovery lifetime. The type S allows for five values of forward and reverse current from 1 mA to 20 mA. Open-circuit decay is simply obtained by a zero reverse current switch position.

A special probe stage was built for the measurement of cells and diodes in wafer form. It incorporated coaxial, shielded leads and a soft (Be-Cu), rounded probe so that shallow junctions could be probed without placing unnecessary pressure on the junction. Micromanipulators on the probe and stage and a mounted microscope allow for alignment of the probe and diode under test.

For the case of small mesa diodes, the diodes were soldered to a standard TO-5 header and a 2-mil-diameter aluminum wire was bonded to the top metallization of the diode. This allowed a direct connection of the TO-5 header to the input of the type S, thereby reducing stray and lead capacitance.

REFERENCES

1. P. A. Iles, Proc. 9th Photovoltaic Specialists Conf., p. 15, May 1972.
2. H. W. Brandhorst, Jr., Proc. 9th Photovoltaic Specialists Conf., pp. 37-43, May 1972.
3. J. Lindmayer and J. Allison, COMSAT Technical Rev. 3, 1 (1973).
4. V. L. Dalal, H. Kressel, and P. H. Robinson, J. Appl. Phys. 46, 1283 (1975).
5. J. Mandelkorn, J. H. Lamneck, and L. R. Scudder, Proc. 10th Photovoltaic Specialists Conf., pp. 207-211, November 1973.
6. H. W. Brandhorst, Jr., C. R. Baraona, and C. K. Swartz, Proc. 10th Photovoltaic Specialists Conf., pp. 212-216, November 1973.
7. M. Wolf, Proc. 10th Photovoltaic Specialists Conf., pp. 5-14, November 1973.
8. F. A. Lindholm, S. S. Li, and C. T. Sah, Proc. 11th Photovoltaic Specialists Conf., pp. 3-12, (1975).
9. W. Shockley, Bell Syst. Tech. J. 28, 435 (1949).
10. M. P. Godlewski, C. R. Baraona, and H. W. Brandhorst, Jr., Proc. 10th Photovoltaic Specialists Conf., pp. 40-49, November 1973.
11. J. G. Fossum, Intl. Electron Devices Meeting, Washington, DC, December 13, 1975.
12. J. Mandelkorn and J. H. Lamneck, Proc. 11th Photovoltaic Specialists Conf., pp 36-39, (1975).
13. W. Kern and D. A. Puotinen, RCA Review 31, 187 (1970).
14. R. G. Mazur and D. H. Dickey, J. Electrochem. Soc. 113, 255 (1966).
15. R. G. Mazur, Proc. Spreading Resistance Symposium, NBS special publication 400-10, pp. 5-15, December 1974.
16. R. L. Meek, T. E. Seidel, and A. G. Cullis, J. Electrochem. Soc. 122, 786 (1975).
17. H. F. Wolf, *Silicon Semiconductor Data*, Vol. 9, (Pergamon Press, London, 1969), pp. 500-504.
18. M. Wolf, Proc. IEEE 51, 674 (1963).
19. D. A. Kleinman, Bell Syst. Tech. J. 40, 85 (1961).
20. B. Ellis and T. S. Moss, Solid State Electronics 13, 124 (1970).

21. N. Goldsmith, R. V. D'Aiello, and R. A. Sunshine, Proc. Spreading Resistance Symposium, in NBS special publication 400-10, pp. 223-234, December 1974.

22. M. P. Godlewski, H. W. Brandhorst, Jr., and C. R. Baraona, Proc. 11th Photovoltaic Specialists Conf., p. 3235, 1975.

23. S. R. Lederhandler and L. J. Giacoletto, "Measurement of Minority Carrier Lifetime and Surface Effects in Junction Devices," Proc. IRE 43, 478 (1955).

24. H. J. Kuno, "Analysis and Characterization of P-N Junction Diode Switching," IEEE Trans. Electron Devices ED-11, 8 (1964).